PP1 initiates the dephosphorylation of MASTL, triggering mitotic exit and bistability in human cells

Samuel Rogers[1], Dirk Fey[2], Rachael A. McCloy[1], Benjamin L. Parker[3], Nicholas J. Mitchell[4], Richard J. Payne[4], Roger J. Daly[5], David E. James[3], C. Elizabeth Caldon[1,6], D. Neil Watkins[1,6,7], David R. Croucher[1,6] and Andrew Burgess[1,6]

1. The Kinghorn Cancer Centre, Garvan Institute of Medical Research, Darlinghurst, NSW, 2010, Australia.
2. Systems Biology Ireland, University College Dublin, Dublin, Ireland
3. The Charles Perkins Centre, School of Molecular Bioscience and Sydney Medical School, The University of Sydney, NSW 2006, Australia.
4. School of Chemistry, The University of Sydney, Sydney, NSW, Australia
5. Department of Biochemistry and Molecular Biology, School of Biomedical Sciences Monash University, Clayton, VIC, 3800, Australia
6. St. Vincent's Clinical School, Faculty of Medicine, UNSW, Darlinghurst, NSW, Australia
7. Department of Thoracic Medicine, St Vincent's Hospital, Darlinghurst, NSW, 2010.

Keywords: Mitotic Exit, Greatwall, MASTL, PP1, PP2A, Cdk1, kinase, phosphatase, bistable switch

Correspondence to be addressed to:
Email: a.burgess@garvan.org.au

Summary Statement

Our results show that loss of Cdk1 activity allows PP1 to partially dephosphorylate MASTL, activating PP2A, which completes the dephosphorylation and deactivation of MASTL, thereby promoting mitotic exit.

Abstract

Entry into mitosis is driven by the phosphorylation of thousands of substrates, under the master control of Cdk1. During entry into mitosis, Cdk1, in collaboration with MASTL kinase, represses the activity of the major mitotic protein phosphatases, PP1 and PP2A, thereby ensuring mitotic substrates remain phosphorylated. For cells to complete and exit mitosis, these phosphorylation events must be removed, and hence, phosphatase activity must be reactivated. This reactivation of phosphatase activity presumably requires the inhibition of MASTL, however, it is not currently understood how or what deactivates MASTL. In this study, we identified that PP1 is associated with and capable of partially dephosphorylating and deactivating MASTL during mitotic exit. Using mathematical modelling we were able to confirm that deactivation of MASTL is essential for mitotic exit. Furthermore, small decreases in Cdk1 activity during metaphase are sufficient to initiate the reactivation of PP1, which in turn partially deactivates MASTL to release inhibition of PP2A and hence create a feedback loop. This feedback loop drives complete deactivation of MASTL, ensuring a robust switch-like activation of phosphatase activity during mitotic exit.

Introduction

The phosphorylation of proteins by Cyclin dependent kinase 1 (Cdk1) is essential for correct entry into and progression through mitosis (Lindqvist et al., 2009). Cdk1 substrates directly and indirectly ensure that the DNA is correctly compacted into chromosomes, and positioned at the centre of the cell by bi-polar attachment to the mitotic spindle. This process is monitored by the spindle assembly checkpoint (SAC), which ensures that Cdk1 remains active until all chromosomes are correctly attached and aligned. Once this is achieved, the SAC becomes satisfied, releasing inhibition of the E3 ubiquitin ligase APC^{cdc20}, which targets Cyclin B1 for destruction by the proteasome, inactivating Cdk1 (Wolf et al., 2006). To exit mitosis, phosphatases reverse the Cdk1-dependent phosphorylation events. Notably, phosphatases are inhibited by Cdk1 activity, consequently inactivating Cdk1 creates a negative feedback-loop enhancing phosphatase activity, locking the system into irreversible mitotic exit (Yang and Ferrell, 2013). Differentially oscillating activities of Cdk1 and phosphatase activity create a two-state system; interphase and mitosis respectively (Medema and Lindqvist, 2011). This bistability has been extensively modelled mathematically, especially with regards to the role of Cdk1, and protein degradation during mitotic exit (López-Avilés et al., 2009; Rattani et al., 2014; Tóth et al., 2007). Consequently, how regulation of Cdk1 activity ensures the irreversibility of mitotic exit is now well established.

Recent studies have focussed on how regulating phosphatases impacts on bistability during mitosis. In yeast, Cdc14 is the primary phosphatase responsible for counter-balancing Cdk1 (Bouchoux and Uhlmann, 2011), however, in human cells it does not appear to play a central role (Mocciaro and Schiebel, 2010). Consequently, in higher eukaryotes its unclear which phosphatase/s regulate mitotic exit. In cycling *Xenopus* extracts, depleting PP1 prevents the dephosphorylation of mitotic substrates (Wu et al., 2009), while Cdk1-mediated phosphorylation on Thr320 of PP1 inhibits its activity (Kwon et al., 1997). However, PP2A-B55 is also proposed as the major Cdk1 counterbalancing phosphatase during mitotic exit in both Xenopus (Mochida et al., 2009) and human systems (Schmitz et al., 2010). PP2A-B55 must be inhibited during mitotic entry to ensure that Cdk1 substrates remain phosphorylated during mitosis, and subsequently reactivated upon exit. This mitotic inhibition of PP2A-B55 is under the control of microtubule associated serine-threonine like kinase (MASTL) (Burgess et al., 2010; Vigneron et al., 2009). MASTL, originally identified in *Drosophila* as Greatwall (Gwl) (Bettencourt-Dias et al., 2004), is phosphorylated (most likely by Cdk1) on

several key residues (Thr194, Thr207, S213 and Thr741), followed by auto-phosphorylation on Ser875 (Blake-Hodek et al., 2012). Active MASTL then phosphorylates two homologous heat-stable proteins alpha-endosulfine (ENSA) (Ser67) and Arpp19 (Ser62) (Gharbi-Ayachi et al., 2010; Mochida et al., 2010), which then bind to the active site of PP2A-B55 acting as an 'unfair' competitive inhibitor (Williams et al., 2014). To exit mitosis, Cdk1 substrates must be dephosphorylated; presumably this requires the deactivation of MASTL, releasing ENSA mediated repression of PP2A-B55 activity. Interestingly, PP2A-B55 has recently been proposed to dephosphorylate MASTL during mitotic exit (Hégarat et al., 2014), however, as PP2A is inhibited by MASTL, an external trigger is likely required to initiate the deactivation of MASTL to kick-start PP2A activity. Here we demonstrate that PP1 is associated with MASTL during mitotic exit, and capable of dephosphorylating MASTL, correlating with its deactivation. Mathematical modelling showed that PP1 is required for triggering the initial dephosphorylation of MASTL, releasing PP2A inhibition, which completes MASTL and Cdk1 substrate dephosphorylation. In summary our data provides a unifying theory where both PP1 and PP2A are required for efficient deactivation of MASTL thereby establishing a bistable switch that drives mitotic exit.

Results

Biochemical modelling of mitotic exit in human cells.

To analyse how MASTL is deactivated during mitotic exit, we utilised highly enriched cultures of mitotic human (HeLa) cells similar to the one we and others have used previously (Cundell et al., 2013; Hégarat et al., 2014; McCloy et al., 2014). Briefly, thymidine synchronised cells were released into nocodazole, with prometaphase cells enriched by gentle mitotic shake-off. The Cdk1 inhibitor RO3306 was then added to induce synchronised mitotic exit (Fig. 1A). To validate the synchronised mitotic exit in our model, the APC^{cdc20} substrates securin and Cyclin B1 were analysed by western blotting. Securin was rapidly degraded within 5 min while Cyclin B1 was slowly degraded throughout the time course, reaching interphase levels at approximately 60-90 min post Cdk1 inhibition, indicating that cells had completed mitotic exit by this time (Fig. 1B). Dephosphorylation of mitotic Cdk1 substrates was analysed using phospho-specific antibodies for proline-directed phospho-threonine (pThrCdk) and phospho-serine (pSerCdk) sites. Significant dephosphorylation of pThrCdk sites was observed within 5 min of RO3306 addition, while pSerCdk sites occurred with slower, linear-like kinetics (Fig. 1C), similar to Cyclin B1 degradation (Fig. 1B). This preferential dephosphorylation of pThrCdk substrates mirrors our previous reports on the differential dephosphorylation patterns that occur during mitotic exit (McCloy et al., 2015). Taken together, these results indicate our system is capable of modelling and temporally separating the early events of mitotic exit, such as chromosome segregation (securin degradation) and the preferential dephosphorylation of pThrCdk substrates, from later events, such as chromosome decondensation and dephosphorylation of pSerCdk substrates.

Previous reports indicate that MASTL activity is primarily regulated through phosphorylation (Burgess et al., 2010), however degradation of the K71M mutant of MASTL has been reported in *Xenopus* oocytes (Yamamoto et al., 2011), and HSP90 depletion destabilises MASTL (Yamamoto et al., 2014). Therefore, to determine if degradation contributes to the regulation of MASTL during mitotic exit, total protein levels were quantified either in the presence or absence of the proteasome inhibitor MG132. Treatment with MG132 successfully blocked Cyclin B1 degradation for the length of the time course (Fig. 1D), however, no significant change in MASTL levels in the presence or absence of MG132 were observed, indicating that degradation does not play a role in regulating MASTL during mitotic exit (Fig.1D). In contrast, potential dephosphorylation of MASTL, as indicated by a band-shift, was noticeable within 10 min, independent of proteasome inhibition. This

dephosphorylation of MASTL, was also observed in MCF10A and MDA-MB-157 human cell lines (Fig. 1E), indicating that dephosphorylation is likely the primary mode of regulating MASTL during mitotic exit in human cells.

Therefore, we next analysed the kinetics of MASTL dephosphorylation and kinase activity. Within 5 min of triggering mitotic exit, a decrease in MASTL mobility shift was observed, which continued step-wise until 90 min where migration matched that of interphase cells, indicating complete dephosphorylation (Fig. 1F). Surprisingly, despite this step-wise dephosphorylation, significant loss of kinase activity, as determined by *in vitro* kinase assays, was observed within 5 min of triggering mitotic exit (Fig. 1F). In contrast, Cdk1/Cyclin B1 *in vitro* kinase activity showed a slow linear decline throughout the time course (Fig. 1F), which correlated with the degradation of Cyclin B1 (Fig. 1B). Taken together, these results suggest that a subset of key phosphorylation sites within MASTL are dephosphorylated initially, causing a small increase in mobility by band-shift, and a significant decrease in kinase activity.

Analysis of MASTL phosphorylation sites during mitotic exit

Human MASTL has 50 reported phosphorylation sites in the PhosphoSitePlus database (http://www.phosphosite.org/), however in Xenopus only Thr194, Thr207, Ser213, Thr741 and Ser885 appear to be critical for kinase activity (Blake-Hodek et al., 2012). To analyse the dephosphorylation of human MASTL during mitotic exit, we mined our recent publication of the global phosphoproteomic mapping of early mitotic exit for MASTL phosphosites (McCloy et al., 2015). This large dataset identified 18 mitotic phosphorylation sites on MASTL and all contained quantitative $\log_2$ scores, with the exception of Ser875, which due to the cleavage site of trypsin, did not contain any heavy isotope residues (Fig. 2A). The majority of sites showed a four-fold decrease in phosphorylation (log2 scores <-2, blue), indicating that they are rapidly dephosphorylated during early mitotic exit, with Ser222, Ser452, Ser660 and Ser668 significantly decreased (adjusted p-values <0.05). The Thr207 site was also rapidly dephosphorylated however, ratios were only found in two of the three biological replicates limiting its significance (p value <0.06).

To analyse the dephosphorylation on MASTL in greater detail, we immunoprecipitated endogenous MASTL using a polyclonal antibody raised against the full length protein from synchronised mitotic extracts (Fig. 2B). These were then probed with a phospho-specific

antibody against the Ser875 auto-phosphorylation site in MASTL (Vigneron et al., 2011). Surprisingly, phosphorylation on Ser875 remained stable throughout mitotic exit, suggesting that this site, although critical for activity, is not involved in regulating the deactivation of MASTL in our system (Fig. 2B). We therefore turned our attention to the other sites in MASTL critical for activity (Thr194, Thr207, Ser213, and Thr741). Unfortunately, we were unable to produce phosphospecific antibodies for these sites. However, all the threonine sites are proline directed and therefore potentially phosphorylated by Cdk1. In support, both the Thr194 and Thr207 site can be phosphorylated by Cdk1 *in vitro* (Blake-Hodek et al., 2012). Given this we reasoned that the pThrCdk substrate antibody could serve as a surrogate marker for these sites. Probing MASTL immunoprecipitations (IPs) with the pThrCdk antibody showed rapid (~50%) reduction in signal within 5 min of triggering mitotic exit, with complete loss by 60 min (Fig. 2B). In contrast, precipitation of the retinoblastoma protein (Rb), a substrate we previously identified to be stably phosphorylated on pThrCdk sites during mitotic exit (McCloy et al., 2015), showed consistent levels of pThrCdk staining throughout the time course. Notably, the Ser780 site on Rb was gradually removed during mitosis (Fig. 2C). Control IPs using a Rabbit IgG antibody did not show any cross-reactive staining for pThrCdk (Fig. 2D). Taken together, these results suggest that the pThrCdk antibody is able to specifically identify phosphosites within MASTL.

To further validate these findings under normal mitotic exit conditions, we utilised in situ Proximity Ligation Assays (PLA), which detects the co-localisation of two proteins within 40nm (Rogers et al., 2015a). Negative control PLA assays using pThrCdk or MASTL antibodies in combination with IgG showed very few interactions, consistent with background levels (Supplementary material Fig. S1A and S1B). Combination of MASTL and pThrCdk antibodies showed a significant increase over background levels, with the number of interactions increasing as cells entered mitosis, peaking during prometaphase, and then declining significantly as cells entered anaphase (Fig. 2E). This dephosphorylation trend paralleled the loss observed by western blot analysis of MASTL IPs (Fig. 2B) and correlated with kinetics of deactivation of kinase activity (Fig. 1F). Hence, the fact that MASTL dephosphorylation occurred concurrently with kinase inactivation, implies that these events may be correlated.

Identification of the phosphatase responsible for deactivating MASTL during mitotic exit

The above results indicate that MASTL activity is regulated by rapid dephosphorylation on key sites during early mitotic exit. To identify the phosphatase responsible for trigging this initial, partial dephosphorylation of MASTL, we precipitated MASTL from cells grown in stable isotope labelling using amino acids in cell culture (SILAC) and then analysed bound proteins by quantitative mass spectrometry. Briefly, cells were cultured for 6-7 doublings in the presence of "heavy" or "light" amino acids, as described previously (McCloy et al., 2015). Cells were then synchronised as per Fig. 1A where "light" samples remained arrested in prometaphase, while "heavy" cultures were treated with RO3306 for 20 min to induce mitotic exit. Endogenous MASTL was IP from both cultures, mixed 1:1, separated by gel electrophoresis, digested in-gel and analysed by LC-MS/MS (Fig. 3A). Importantly, MASTL was highly enriched, with good sequence coverage (44.3%) and significant peptide identification confidence (posterior error probability $2.43E^{-176}$), providing an internal positive control (Fig. 3B). After filtering for contaminants, a total of 753 unique proteins were identified and quantified by mass spectrometry at a 1% false discovery rate (Supplementary material Table S1). Analysis of this dataset revealed 8 phosphatase proteins that were potentially interacting with MASTL during mitotic exit (Fig. 3B). The list contained the scaffolding A and regulatory B55α subunit of PP2A, the regulatory subunit myosin phosphatase MYPT1 (PPP1R12A), and myosin phosphatase Rho interacting protein (MPRIP), along with the catalytic subunits of PP1 (PPP1C- α, β, γ). While all three PP1 isoforms were "detected", the majority (11 out of 14) of peptides identified were not isoform specific. PP1γ, MYPT1, MPRIP and PP2A-B55 displayed slightly increased association with MASTL during mitotic exit (Log_2 ~0.3 to 0.6), while PP1 α and β were slightly reduced. However, these values were all less than 1-fold, well below the standard 2-fold change threshold normally required for relevance. In summary, the higher confidence identification of multiple PP1 family members suggests that PP1 is the potential MASTL phosphatase.

To confirm the above interactions, additional co-IP and western blot analysis was performed. Immunoprecipitation of endogenous MASTL from prometaphase and early mitotic exit samples showed a strong interaction with the catalytic PP1β subunit, which notably increased in the early mitotic exit (+RO) sample (Supplementary material Fig. S1C, IP1). Further depletion of MASTL from the same extracts failed to recapitulate any noticeable association with PP1β (Supplementary material Fig. S1C, IP2). In addition, MASTL was detected, albeit weakly in the reverse PP1β IPs (Supplementary material Fig. S1D). However, depletion of

extracts with a control Rabbit IgG antibody was also able to weakly co-precipitate PP1β during the mitotic exit sample (Supplementary material Fig. S1C). The presence of IgG prevented the analysis of PP2A-A and B55 subunits in MASTL IPs, therefore we probed for the catalytic subunit of PP2A, however, no association was observed, suggesting that PP2A is not strongly associated with MASTL during early mitotic exit events. Taken together, although MASTL and PP1β appear to be associated during mitotic exit, the non-specificity observed with IgG prevents us from concluding this conclusively.

Therefore, to overcome issues associated with non-specific IgG precipitation of PP1, and to validate the interactions under normal mitotic progression, we utilised PLA assays. To ensure specificity of the antibodies used for PLA, siRNA knockdown of MASTL, PP1β, PP2A/C and PP2A-B55 were performed followed by immunofluorescence (IF). Knockdown of each protein clearly reduced the signal observed by IF compared to to the non-targeting controls, indicating that the antibodies specifically recognise their target antigens (Supplementary Material Fig. S2A-F). As a positive control for PLA, Cyclin B1 and Cdk1 were analysed. The number of interactions between CycB-Cdk1 increased as cells entered mitosis, peaking at prometaphase, before significantly declining as cells entered anaphase and telophase, corresponding with the reported cyclic production and destruction of Cyclin B1 in HeLa cells (Fig. 3C) (Chang et al., 2003). An additional control using MASTL mouse (Mo) combined with MASTL rabbit (Rb) antibodies was also performed. The number of interactions between MASTL(Mo)-MASTL(Rb) decreased significantly during prometaphase compared to interphase, and then rose again as cells exited mitosis (Supplementary material Fig S3A). This change is likely due to the reduced ability of the antibodies to fully detect phosphorylated forms of MASTL. Finally, no significant association between IgG+MASTL and IgG+PP1β were observed (Supplementary material Fig. S1A and S3B), indicating that the non-specific interaction between IgG and PP1 was restricted to the IPs. Importantly, PP1β+MASTL PLA assays showed positive interactions that increased significantly as cells progressed from interphase into mitosis, peaking at anaphase, before decreasing in telophase (Fig. 3D). The increase observed in anaphase, although significant, could be due to better antigen retrieval, as noted by the corresponding increase in MASTL(mo)-MASTL(Rb) interactions (Supplementary material Fig. S3A). In contrast, no significant associations between the catalytic or the B55 subunit of PP2A and MASTL were observed by PLA (Fig. 3E, Supplementary material Fig. S3C), indicating that PP2A-B55 is not closely associated with MASTL during mitosis. Taken together, these data indicate that PP1 is associated with

MASTL during early phases of mitotic exit, and hence potentially capable of triggering the dephosphorylation of MASTL.

In vitro and in vivo dephosphorylation of MASTL by PP1

The above data suggests that PP1 has the potential to deactivate MASTL, possibly by dephosphorylating critical Thr194, Thr207, and Thr741 pThrCdk sites during early mitotic exit (Fig. 2A). For this model to hold true, it would require rapid reactivation of PP1 during early mitotic exit, to allow subsequent dephosphorylation of MASTL. To test this, we analysed PP1 auto-dephosphorylation of its inhibitory Thr320 site (Wu et al., 2009) in our synchronised mitotic exit system. Significant loss of Thr320 was observed within 5 min of triggering mitotic exit, with complete dephosphorylation of Thr320 occurring within 60 min (Fig. 4A). Accordingly, rapid dephosphorylation of Histone H3 on Thr3, a known PP1 substrate (Qian et al., 2011), was also observed within 5 min, (Fig. 4A). Taken together, these data indicate that PP1 is activated rapidly upon triggering mitotic exit with RO3306, with the timing correlating with the the dephosphorylation of MASTL.

To examine if PP1 can dephosphorylate MASTL, we performed *in vitro* phosphatase assays on precipitated MASTL. To ensure maximum MASTL phosphorylation cells were treated for 60 min with the PP1/PP2A inhibitor Okadaic Acid prior to harvesting. Precipitated MASTL was then treated without (Control) or with purified PP1α, PP1β or lambda Phosphatase for 15, 30, 45 or 60 min. MASTL remained phosphorylated in control samples throughout the time course (Fig. 4B, Supplementary material Fig S3D), while treatment with lambda phosphatase increased MASTL mobility within 15 min, and almost completely dephosphorylated MASTL by 60 min (Fig. 4B and Supplementary material Fig. S3E). Similarly, treatment with PP1α (Fig. 4B) and PP1β (Supplementary material Fig. S3D) produced a small but noticeable increase in MASTL mobility within 15 min, however, this only slightly increased over the remainder of the time course. This suggests that PP1 specifically targets a subset of the phosphorylated residues on MASTL. In support, PP1α treatment almost completely removed pThrCdk phosphosites within 15 min, while phosphorylation of MASTL on S875 was only partially reduced by after 60 min of treatment with PP1α. Notably, lambda phosphatase efficiently removed both pThrCdk and S875 phosphorylation within 15 min, with near complete dephosphorylation observed after 60 min (Fig. 4B and supplementary material Fig S3E).

The above data indicates that PP1α and PP1β can partially dephosphorylate MASTL *in vitro*. To analyse this *in vivo,* HeLa cells were transfected with siRNA against PP1α or PP1β and the kinetics of MASTL dephosphorylation examined using our synchronised mitotic exit model (Fig. 1A). Knockdown of PP1γ and complete knockdown of PP1α or β caused significant toxicity and inhibited mitotic entry (data not shown). However, sufficient numbers of mitotic enriched cells were obtained with partial (~20-50%) depletion of PP1α or β. Unfortunately, triggering mitotic exit in partially depleted cells with 10 μM of RO3306 had no clear effect on MASTL dephosphorylation kinetics. The lack of *in vivo* effect could be due the potential redundancy between PP1 isoforms, evidenced by both PP1α and PP1β dephosphorylating MASTL *in vitro*. In support, in the sections below we employed mathematical modelling of mitotic exit to guide our experiments, and were subsequently able to observe direct effects of PP1 co-knockdown on MASTL phosphorylation *in vivo*.

Development of a mathematical model of Phosphatase Reactivation during Mitotic Exit

Our data above implicates PP1 as the phosphatase responsible for triggering deactivation of MASTL during mitotic exit. We were unable to confirm this result *in vivo*, most likely because of limitations with sensitivity and toxicity of PP1 knockdown in our mitotic exit system. Therefore, we developed a computational model based on our empirical data, to delineate the minimal requirements needed for triggering PP1 dephosphorylation of MASTL and mitotic exit. A central component for mitotic exit is the presence of a bistable switch (green shading), where the presence of feedback loop/s trigger the transition between two stable states, mitosis (on, red shading) and interphase (off, blue shading) (Verdugo et al., 2013) (Fig. 5A). The core of our model (Fig. 5B, see Fig. S3F for a reaction kinetic scheme) is based on established models of Cdk1, MASTL, ENSA and PP2A. Specifically, our model comprises two feed-forward loops (black lines) from CDK1, the first suppresses the phosphatase activities of PP1 by phosphorylation of Thr320 (Wu et al., 2009) and the second suppresses PP2A via MASTL phosphorylation of ENSA (Gharbi-Ayachi et al., 2010). Two feedback loops (red lines) were also incorporated; a positive feedback loop from PP1 to itself and a double negative feedback loop via inhibition of MASTL and re-activation of PP2A as indicated by our data (Fig. 2 & 3). In the positive loop, PP1 can activate itself through auto-dephosphorylation of its inhibitory Thr320, which is under the control of Cdk1 (Wu et al., 2009). The double negative feedback loop is initiated by the deactivation of MASTL by PP1, which in turn releases PP2A inhibition (Fig. 5B). To close this double feedback loop, we create 2 alternative models (Supplementary material Fig. S3F). The first model (a) was based

on the direct/indirect reactivation of PP1 by PP2A through regulation of MYPT1 (Lontay et al., 2005) and dephosphorylation of inhibitors I-1 and Darpp32 (El-Armouche et al., 2005; Wu et al., 2009). The second model (b), PP2A directly feeds back onto MASTL and is responsible for the removal of additional Cdk1 phosphosites and inhibition of MASTL activity (Hégarat et al., 2014). All equations, reaction values, and estimated parameter values are listed in Supplementary Tables S2-6.

To train these models we utilised the biological data generated from our highly synchronised mitotic exit system detailed above (Fig. 1A-F, 2B, and 4A), combined with the reported published abundance for each protein in HeLa cells from the MOPED database (Kolker et al., 2012), and the reported K*m* and K*cat* values for the dephosphorylation of ENSA by PP2A-B55 (Williams et al., 2014). The remaining dephosphorylation rates were uncertain and thus estimated using model (a) and adaptive simulated annealing, a method for global parameter estimation (Ingber, 1989). To assess the associated uncertainty, a Monte-Carlo based approach was used where the initial parameters were randomly changed 50 times and the model refitted to the experimental data (Hengl et al., 2007; Maiwald and Timmer, 2008). We then analysed parameter correlations and variability of the simulated predictions, and although the exact parameter values were not uniquely identifiable, their estimates occupied highly structured regions in the parameter space resulting in parameter correlations (Supplementary material Fig. S3G).

For model (a), all 50 estimated models (light grey lines), and in particular the best fitting model (solid back line), closely matched our experimental data (red dots) for the kinetics of PP1 inhibition (Thr320 dephosphorylation), MASTL kinase activity, and the dephosphorylation of global pThrCdk sites, a readout of PP2A reactivation and mitotic exit (Fig. 5C). Using the same parameter estimates, model (b) was also able to closely match our experimental data in 60% of the simulations (Fig. 5D). This indicates that the differences between model (a) and (b) are not critical for explaining these data, and therefore for simplicity we choose model (a) for further analysis.

Validation of the model

One limitation of the above simulations and our biological system is that they relied on instantaneous inhibition of Cdk1. Therefore, our first simulation was to test whether bistable,

switch-like dynamics would be maintained if Cdk1 activity declined gradually, similar to normal degradation of Cyclin B1. Simulating the model with two different decay rates of Cdk1 activity delayed the onset of mitotic exit (Fig. 6A). Importantly, this delay did not alter the switch-like behaviour with regards to PP1 inhibition, deactivation of MASTL and subsequent dephosphorylation of pThrCdk substrates, which all occurred with similar kinetics to instantaneous Cdk1 inhibition. This indicates that Cdk1 activity determines the timing of mitotic exit, and once Cdk1 activity drops below a certain threshold, the bistable phosphatase switch is triggered and mitotic exit occurs. Therefore, our method of instantaneous Cdk1 inhibition is a useful method for modelling mitotic exit.

Next we utilised the model to determine the threshold of Cdk1 activity that triggers the bistable switch and mitotic exit. Surprisingly, the model identified a clear bistable threshold, with 90% or greater inhibition of Cdk1 required to trigger PP1 activation, MASTL and pThrCdk substrate dephosphorylation (Fig. 6B). To validate this experimentally, increasing doses of RO3306 were added to nocodazole arrested cells for 30 min. No significant effect on the dephosphorylation of MASTL (as determined by band-shift), was observed below 1 μM of RO3306 (Fig. 6C). A small increase in MASTL mobility and dephosphorylation of PP1 on Thr320 was observed at 3 μM, which became clear and significant at 5 μM. Notably, a dose of 5μM has been reported to inhibit up to 90% of Cyclin B-Cdk1 activity (Vassilev et al., 2006), matching the predictions made by our model.

Based on these data, we hypothesised that sub-optimal doses of RO3306 at the switching threshold for Cdk1, might allow subtle changes in MASTL dephosphorylation to be observed with siRNA depletion of PP1. To test this, we repeated the partial knockdown of PP1α and β and then treated cells with 1-5 μM RO3306 for 30 min. No clear effect was seen when PP1α or β were depleted individually (Supplementary material Fig. S4A), however, partial co-depletion of PP1α and β produced a small but noticeable increase in the slower migrating form of MASTL at both 1 and 3 μM (Fig. 6D). This corresponded with a slight increase in the amount of histone H3 Thr3 phosphorylation levels, indicating that PP1 was partially inhibited. Taken together these data suggest PP1 is capable of directly regulating the dephosphorylation of MASTL during mitotic exit. Furthermore, there is some redundancy between PP1 α and PP1β, which likely explains why we failed to observe any effect in single knockdown experiments.

To further validate PP1 dephosphorylation of MASTL *in vivo*, we employed a novel peptide activator (PDP3) of PP1 (Chatterjee et al., 2012). Treatment of enriched prometaphase arrested cells with PDP3 induced a small (~20%) decrease in pThr320 phosphorylation on PP1. This corresponded with significant dephosphorylation on histone H3-Thr3 indicating that PP1 is reactivated by the peptide (Fig. 6E). To estimate the level of MASTL dephosphorylation, we compared the ratio between phosphorylated upper band (green) and dephosphorylated lower (red) migrating bands. The levels of MASTL dephosphorylation of closely matched Thr320 dephosphorylation PP1 reactivation, with treatment with PDP3 alone inducing a ~20% increase in MASTL mobility. Interestingly, this partial ~20% activation of PP1 and inhibition of MASTL did not trigger mitotic exit, with PP2A substrates (pThrCdk and pThr481-PRC1) remaining phosphorylated (Fig. 6E and Supplementary Material Fig. S4B). Next we hypothesised that combination of PDP3 with partial inhibition of Cdk1 just below the bistability threshold might trigger mitotic exit. Addition of 3 μM RO3306 reduced pThr320 phosphorylation on PP1 by ~50%, which when combined with PDP3 reduce to ~75% of control levels and resulted in a near complete dephosphorylation of pThr3-H3. MASTL dephosphorylation matched PP1 reactivation, with RO treatment increasing mobility by ~50%, while PDP3 in combination with RO and PDP3 reduced phosphorylation by ~75% (Fig. 6E). Surprisingly, while addition of 3 μM RO did increase the dephosphorylation of pThrCdk and pThr481-PRC1 over PDP3 alone, the combination of PDP3 and RO did not significantly increase dephosphorylation further (Fig. 6E and Supplementary Material Fig. S4B), indicating that PP2A remained partially inhibited under these conditions. This data was used to update all the parameter estimations in our mathematical model (Supplementary material Fig. S4C). Importantly, introduction of partial (20-40%) activation of PP1 and subsequent MASTL deactivation, corresponded with a similar partial dephosphorylation of pThrCdk substrates, but did not trigger the bistable mitotic exit switch (Supplementary material Fig. S4D). Furthermore, this revised model (a rev) was still able to accurately model our experimental data based on rapid (90%) Cdk1 inhibition (Supplementary material Fig. S4E). Notably, previous reports in *Xenopus* cell free extracts have indicated that as little as ~30% of MASTL activity is sufficient for maintaining phosphorylation of mitotic substrates (Blake-Hodek et al., 2012; Vigneron et al., 2011), which likely explain why partial dephosphorylation and deactivation of MASTL by PP1 is insufficient to drive mitotic exit by itself.

MASTL deactivation is essential for mitotic exit and requires both PP1 and PP2A

A major hypothesis of this work is that MASTL must be deactivated to permit mitotic exit. In support, we have previously shown in *Xenopus* extracts that the mitotic state is lost upon depletion of MASTL, even when Cdk activity is maintained (Vigneron et al., 2009). However, to date no one has been able to produce a constitutively active form of MASTL with which to validate this hypothesis. Therefore, we introduced a constitutive active form of MASTL into our model. Interestingly, this completely prevented exit and bistability (Fig. 7A). Similarly, complete removal of the auto-dephosphorylation loop on PP1 was sufficient to prevent the bistable switch at the estimated Cdk1 inhibitor effectiveness (dCdk1=0.911) (Fig. 7B, red line). To examine the dynamics of MASTL deactivation by PP1 in more detail, we simulated the effects on MASTL deactivation with increasing levels of PP1 inhibition. Increasing inhibition of PP1 from 30-70% caused incomplete deactivation of MASTL and dephosphorylation of pThrCdk substrates without significantly affecting the shape of the response (Fig. 7B and 7C). However, to completely prevent MASTL deactivation and block mitotic exit >90% of PP1 inhibition was required (Fig. 7A and Fig. 7B light green line). Further, the response to PP1 inhibition is gradual, resembling a linear rather than an ultrasensitive switch-like curve, hence there is no pronounced threshold at which mitotic exit is prevented. Further explaining why partial siRNA depletion or reactivation of PP1 with PDP3 only had a small effect on MASTL dephosphorylation. Therefore, we next examined the impact that PP2A has on MASTL deactivation and bistability in our model. In contrast to PP1, the PP2A response was highly nonlinear and switch-like. Partial inhibition of PP2A (30%, dark blue line) significantly delayed the kinetics of mitotic exit, and the bistable switch was completely abolished at 50% inhibition of PP2A (light blue line) (Fig. 7D and 7E). This non-linear, switch-like response indicates that the feedback loop from PP2A to PP1 (and/or MASTL) is critical for generating the required ultra-sensitivity. To validate this prediction, we took advantage of the 10-100 fold differential selectivity of Okadaic Acid (OA) for PP2A over PP1 (Swingle et al., 2007), with doses below 1 μM reported to be specific for PP2A in human cell lines (Favre et al., 1997). Prometaphase enriched HeLa cells were exposed to increasing doses of OA (0-2000 nM) prior to triggered mitotic exit with RO3306. Based on our model, mitotic exit and MASTL dephosphorylation should be rescued when >50% inhibition of PP2A is achieved. In agreement, rescue of MASTL and global pThrCdk phosphorylation was observed at 50-100 nM with near complete rescue observed at 500 nM of OA (Fig. 7E). In contrast, a dose of 1-2000 nM was required to rescue the auto-

dephosphorylation of PP1 on Thr320 and significantly increase pThr3-H3 levels, indicating substantial PP1 inhibition. Interestingly, these high doses were able to further increase the band shift observed for MASTL further supporting the role of PP1 triggering a partial dephosphorylation of MASTL.

To test the importance of PP1 on MASTL dephosphorylation, we created a final alternative model (c), where the negative feedback from PP1 to MASTL was removed, but feedback from PP2A to MASTL and PP1 remained (Fig. 7G). This alternative model (black lines) closely matched our experimental data (blue dash lines) for the dephosphorylation of PP1 observed upon inhibition of Cdk1 (Supplementary material Fig. S4F). However, it was not able to model the dephosphorylation of MASTL or pThrCdk substrates, which remained stable (Fig. 7H, blue dashed lines). Artificially increasing dephosphorylation rate (k4) of MASTL ten-fold allowed the alternative (c) model to fit the experimental results for MASTL and pThrCdk dephosphorylation (Fig. 7H, black lines). However, when we tested the model using increasing activation of PP1 (20- 80%), instead of Cdk1 inhibition, there was no effect on MASTL dephosphorylation, or pThrCdk substrates (Fig. 7I). Therefore, even under these artificial conditions with highly unstable phosphorylation of MASTL, PP1 is still absolutely required to initiate the dephosphorylation of MASTL, ensuring sufficient reactivation of PP2A, which then triggers the rapid bistable mitotic exit switch.

Discussion

Our results show rapid dephosphorylation and deactivation of MASTL is critical for ensuring bistability during mitotic exit. We propose that PP1 initiates the dephosphorylation of MASTL, relieving the inhibition of PP2A, which then completes the full deactivation of MASTL. The degradation of Cyclin B, which begins during metaphase (Gavet and Pines, 2010), initiates mitotic exit, as decreasing levels of Cyclin B are likely sufficient to relieve Cdk1 phosphorylation of Thr320 on PP1, allowing auto-dephosphorylation and activation. Thus, we believe that our model of bistable phosphatase reactivation, works in combination with the established bistable models of mitotic exit (López-Avilés et al., 2009; Yang and Ferrell, 2013), and collectively ensure the ultra-sensitivity and irreversibility of the mitotic exit switch.

Recent reports in fission yeast demonstrate partial reactivation of PP1 is required for subsequent PP2A-B55 and PP2A-B56 reactivation during mitotic exit. Although the mitotic exit roles of PP1 and PP2A in yeast and humans are not entirely conserved, this relay switch appears to be maintained (Grallert et al., 2014). Furthermore, human cells depleted of PP2A-B55 delay during anaphase rather than metaphase, with defects in post-mitotic spindle breakdown and nuclear envelope reassembly (Schmitz et al., 2010). If PP2A was responsible for the initial dephosphorylation of MASTL, then an earlier metaphase arrest similar to non-degradable Cyclin B would be expected (Chang et al., 2003). This interdependence of PP1 and PP2A for bistability in our model also provides an explanation for previous reports that PP2A dephosphorylates MASTL during mitotic exit (Hégarat et al., 2014). In our model, PP2A is part of the ultra-sensitive feedback loop regulating PP1/MASTL and is needed for establishing bistability. Consequently, partial inhibition of PP2A is sufficient to disrupt PP1 reactivation, block Cdk1 substrate dephosphorylation, thereby maintaining MASTL activity, and preventing mitotic exit. This accounts for the ability of the phosphatase inhibitor OA to rescue MASTL phosphorylation and block mitotic exit at doses specific for PP2A. Additionally, our data showed that >90% of PP1 needs to be inhibited to maintain complete phosphorylation of MASTL and pThrCdk substrates. This likely explains why complete depletion of PP1 prevents Cdk1 substrate dephosphorylation and blocks mitotic exit in Xenopus extracts (Wu et al., 2009). In contrast, inhibitors such as tautomycin, are unlikely to achieve this level of inhibition in human cells (Favre et al., 1997), explaining why these experiments have failed.

The final question remaining is how ~~does~~ PP1 initiates the deactivation of MASTL? We believe that PP1 dephosphorylates key pThrCdk residues (Thr194, Thr207 and Thr741), initiating MASTL deactivation. In support, mutating these sites to non-phosphorylatable Ala mutants reduces MASTL kinase activity by up to 75%, triggering mitotic exit in *Xenopus* extracts (Blake-Hodek et al., 2012). In addition, Thr207 matches the TPG motif, which we previously identified as a highly unstable phosphorylation motif (McCloy et al., 2015). Similarly, dephosphorylation of Thr194 during mitotic exit has also been observed in a similar model of mitotic exit (Hégarat et al., 2014). While preparing this manuscript, Heim *et al*. demonstrated in *Xenopus* extracts that MASTL was also dephosphorylated by PP1. Using several elegant experiments using a mutant (G41S), which lacks auto-phosphorylation ability they proposed that the S883 site (equivalent to S875 in human MASTL) was dephosphorylated by PP1 (Heim et al., 2015). However, this mutant, which appears to act as a dominant negative (Vera et al., 2015), was only partially phosphorylated during mitosis and phosphorylation changes on Ser883 were not directly assessed. In contrast, we did not observe any significant decrease during mitotic exit using a phospho-specific antibody for human Ser875, although PP1 could partially dephosphorylate this site *in vitro*. A likely explanation for these differences is that PP1 could target multiple sites on MASTL during early mitotic exit providing multiple different steady-states of MASTL (Thomson and Gunawardena, 2009). These multiple sites could be targeted by different PP1 isoforms, explaining the redundancy we observed between α and β isoforms. In addition, PP1γ, which we also identified by mass spectrometry, may also be involved in regulating MASTL. Consequently, future studies will be needed to identify the specific phosphosites that are regulated by the various PP1 and PP2A complexes to fully understand how these phosphatases regulate MASTL and ultimately mitotic exit in human cells.

In summary, we believe that our model provides an attractive unifying theory where mitotic exit is triggered by an initial loss of Cdk1 activity during late metaphase, allowing PP1 to begin the dephosphorylation of MASTL, thereby releasing PP2A inhibition and triggering the bistable switch that locks cells into the mitotic exit pathway.

Materials and Methods

Antibodies, Chemicals and Reagents

All antibodies used are listed in Supplementary Material Table S7. MASTL rabbit polyclonal and phosphospecific S875 antibodies generated as previously described (Burgess et al., 2010; Vigneron et al., 2011). RO3306 (Axon MedChem), Okadaic Acid sodium salt (A.G. Scientifix), Nocodazole (Sigma), Thymidine 2'-Deoxycytidine hydrate (Santa Cruz Biotechnology), Protease Inhibitor Cocktail (PIC) (Sigma), Adenosine 5'-triphosphate (New England Biolabs), (*S*)-MG132 (Cayman Chemicals), Iodoacetimide (Sigma), and TCEP-hydrochloride (ThermoFisher Scientific). PDP3 peptide (Reither et al., 2013) was synthesised using H-Rink Amide ChemMatrix resin at a loading of 0.52 mmol/g. Automated and manual solid-phase peptide synthesis (SPPS), preparative and analytical HPLC and analytical LC-MS was performed as described (Mitchell et al., 2015).

Cell culture and synchrony

All cell lines were validated >90% match at CellBank Australia or ATCC using STR profiling, and grown as previously described (Browne et al., 2013). HeLa cells werer synchronised as previously described (McCloy et al., 2015) For mitotic exit synchrony, cells were treated with 10 μM RO3306.

siRNA Design and Transfection.

The Promega T7 Ribomax Express RNAi system was used to produce *in vitro* transcribed siRNAs against CDS target sequences for MASTL (pool) 647-GCTCGTTGGGATTTAACAC, 1144-GGACGCTCTTGTGTAAACC 1879-GCTGTACAAGAGAGTAACC; PP1α 180-GATCTGCGGTGACATACAC; PP1β 619-GATCCAGATAAGGATGTGC; PP2A/C 784-GCTCCAAACTATTGTTATC; PP2A-B55 1297-GTAGCTACTACAAACAATC; non-targeting control (NT)-GGATTGTGCGGTCATTAACTT. Transfection of siRNA was performed using Lipofectamine 3000 Reagent (Invitrogen) as per manufacturer's instructions.

Western Blot, Immunoprecipitation, Phosphatase and Kinase Assays

Western blots were performed and quantified as previously described (McCloy et al., 2014; McCloy et al., 2015). For Immunoprecipitations, protein A/G magnetic beads (Pierce) were mixed with antibodies for 1.5-2 h at RT prior to addition to, lysates for 2 h at RT. For *in vitro*

phosphatase assays, prometaphase enriched HeLa cells were treated with 100 nM Okadaic acid for 1 h prior to harvesting. Cell pellets were lysed in IP lysis buffer, MASTL immunoprecipitated (250 µg), washed 3x with IP lysis buffer, 3x with 20 mM TRIS (pH 8) and resuspended in 50 µl of 1xNEBuffer for PMP supplemented with 1 mM $MnCl_2$. MASTL IPs were then treated without (Control) or with purified active PP1α (1 unit, NEB, #P0754S), PP1β (0.1 µg, abcam, #ab128551), or Lambda Phosphatase (200 units, NEB, #P0753S) for the indicated times at 30ºC. Reactions stopped with 2x LDS-PAGE buffer with DTT, and then boiled at 95ºC for 5 min. All samples were analysed as per western blot. Co-immunoprecipitation was performed identically except without Okadaic acid. IgG or primary antibody bound beads were mixed with lysates for 16-18 h at 4ºC. In some cases, a second round of depletion was performed (IP2) for 2 h at RT. For MASTL kinase assays mitotic exit and interphase synchronised cells were treated as per the immunoprecipitation protocol. Beads were washed in IP lysis buffer (without NP-40), then kinase reaction buffer (KRB) (20 mM HEPES, 10 mM $MgCl_2$, 0.1 $mgmL^{-1}$ BSA, 1 mM DTT). Beads were resuspended in KRB plus 10 µg myelin basic protein and ATP to a final concentration of 400 µM, incubated for 1 h at 37 ºC and anlyased using Kinase GloMax Luminescence kit (Promega) as per the manufacturers instructions. The values for MASTL activity were normalized to the depletion efficiency of the total MASTL IP.

Immunofluorescence / Proximity Ligation Assay

Immunofluorescence (McCloy et al., 2014), and PLA assays (Rogers et al., 2015a) were performed as previously described. All coverslips were mounted in ProLong Gold (Life technologies) and imaged on a Leica DMI6000 SP8 confocal with a 63x 1.4 lens at 1024x1024 resolution powered by LAS AF v8.0. PLA dots were counted, and annotated using Imaris v8.1 as described previously (Burgess et al., 2012; Rogers et al., 2015a). FIJI/Image J v1.50a and Adobe Photoshop CC 2015 were used for image colouring/overlays.

SILAC Labeling and Mass Spectrometry

HeLa cells were SILAC-labelled as previously described (McCloy et al., 2015), with immunoprecipitation and peptide purification describe as per (Di Virgilio et al., 2013). Mass spectrometry, peptide analysis and bioinformatics was performed as describe (McCloy et al., 2015; Rogers et al., 2015b).

Acknowledgements

We thank Paul Timpson and David Thomas for their helpful comments. Ellen Van Dam and Darren Saunders (Luminescent Kinase GloMax), Thierry Lorca and Anna Castro (full-length and phospho-S875 MASTL antibodies) for their gifts. A.B. and D.R.C are CINSW FRL fellows. This work was supported by the CINSW FRL fellowship ID#10/FRL/3-02, The Patricia Helen Guest Fellowship and the Petre Foundation. The funders had no role in study design, data collection, analysis, decision to publish, or preparation of the manuscript.

Author Contribution

SR performed mitotic exit assays, IPs, kinase assays, MS, IF and PLA assays, and co-wrote manuscript. RM, CEC, DNW, NJM and RJP assisted with generating data. BLP, RJD and DEJ assisted with mass spectrometry. DF, with DRC, constructed and analysed the mathematical model. AB performed *in vitro* phosphatase assays, performed data analysis, conceived, designed and wrote the manuscript.

Figures

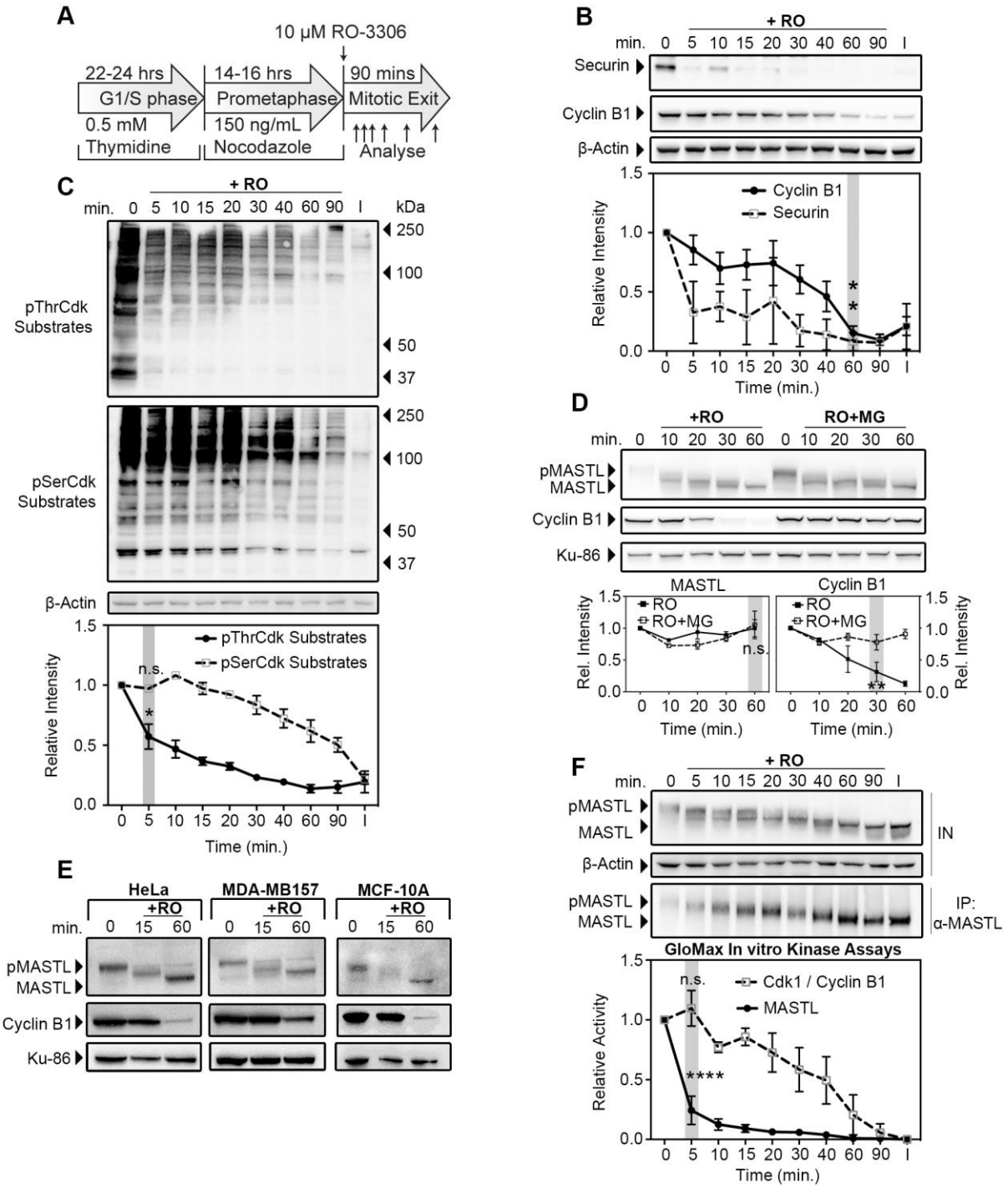

Figure 1. Mitotic exit within human cells is accompanied by rapid dephosphorylation and deactivation of MASTL. **[A]** Schematic method used to generate synchronised mitotic exit in human cells. **[B, C]** HeLa cells synchronised as per A, were lysed and analysed by

western blot for Securin, Cyclin B1, pThrCdk Substrates, pSerCdk Substrates, and β-actin (loading), I = interphase. Quantification is expressed relative to the 0 min. time point (mean + s.e.m.) for n = 3 values, (one-way ANOVA). **[D]** HeLa cells synchronised as per A, were treated with 25 μM of the proteasome inhibitor MG-132 (RO+MG) or without (+RO) for 15 min prior to RO addition. Lysates were blotted for MASTL, where phosphorylated MASTL (pMASTL) and dephosphorylated MASTL (MASTL) are indicated by band shift, Cyclin B1 and Ku-86 (loading). Quantification is expressed as relative to 0 min. time point (mean + s.e.m.) for n=3, (analysis by two-way ANOVA). **[E]** HeLa (cervical), MDA-MB-157 (breast), and MCF-10A (breast) epithelial cells were treated as 1A. Lysates were immunoblotted for MASTL, Cyclin B1 and Ku-86 (loading). **[F]** HeLa cells synchronised as 1A. Cyclin B1 and MASTL were immunoprecipitated (IP) from clear lysates (IN) and then immunoblotted, or assayed using a GloMax Luminescence Kinase Assay kit. Quantification of MASTL and Cdk1 activity are expressed relative to the 0 min time-point, corrected to interphase (mean + s.e.m.), n=3 (one-way ANOVA). Grey shading indicates significant points, P-values, *=<0.05, **=<0.01, ****=<0.0001, and n.s.= not significant.

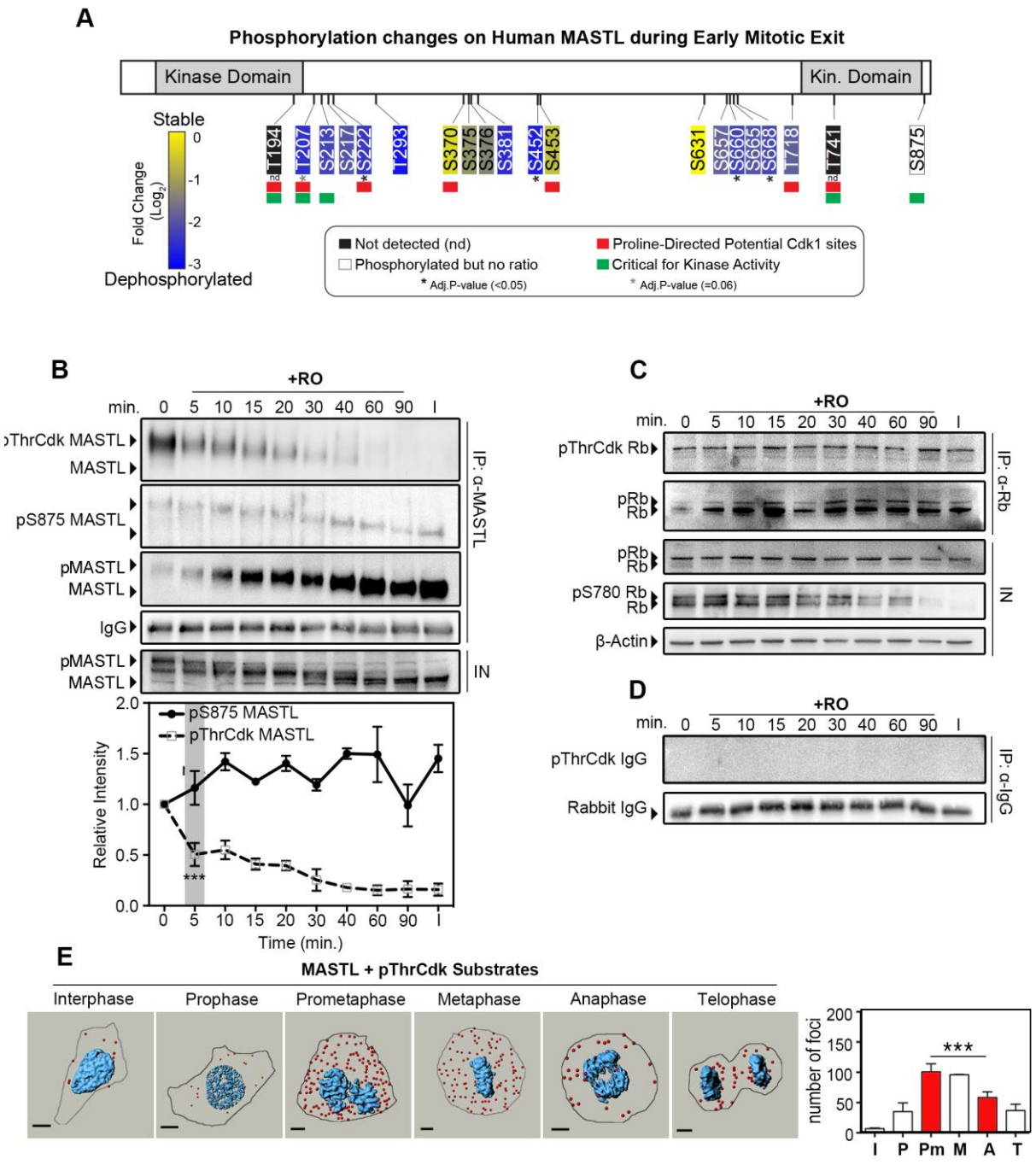

Figure 2. Thr Cdk1 phosphorylations on MASTL are removed during early mitotic exit. **[A]** Summary of MASTL phosphorylation changes during early mitotic exit determined by SILAC mass spectrometry. Shown are sites critical for kinase activity (green), proline directed potential Cdk1 sites (red), and significantly dephosphorylated sites (*). **[B]** MASTL was immunoprecipitated from extracts as in Fig. 1B, immunoblotted with pan-MASTL, pThrCdk substrates (pThrCdk MASTL), and MASTL phosphorylated on S875 (pS875

MASTL). Quantification relative to the 0 min time point, normalised to IgG loading $n = 3$, P-values ***=<0.001, n.s.= not significant (one-way ANOVA). **[C]** Similar to 2B, retinoblastoma protein (Rb) was immunoprecipitated (IP: α-Rb), blotted for total Rb or pThrCdk substrates (pThrCdk Rb); total lysates blotted for Rb phosphorylated on S780 (pS780 Rb), and β-actin (loading). **[D]** IgG precipitation controls corresponding to 2B and C. **[E]** Proximity ligation assay (PLA) using primary antibody pairs of MASTL & pThrCdk (expressed as mean + s.e.m.), for minimum 5 cells, n=2. Prometaphase and anaphase were compared (red bars) P-value ***=<0.001 (two-way ANOVA).

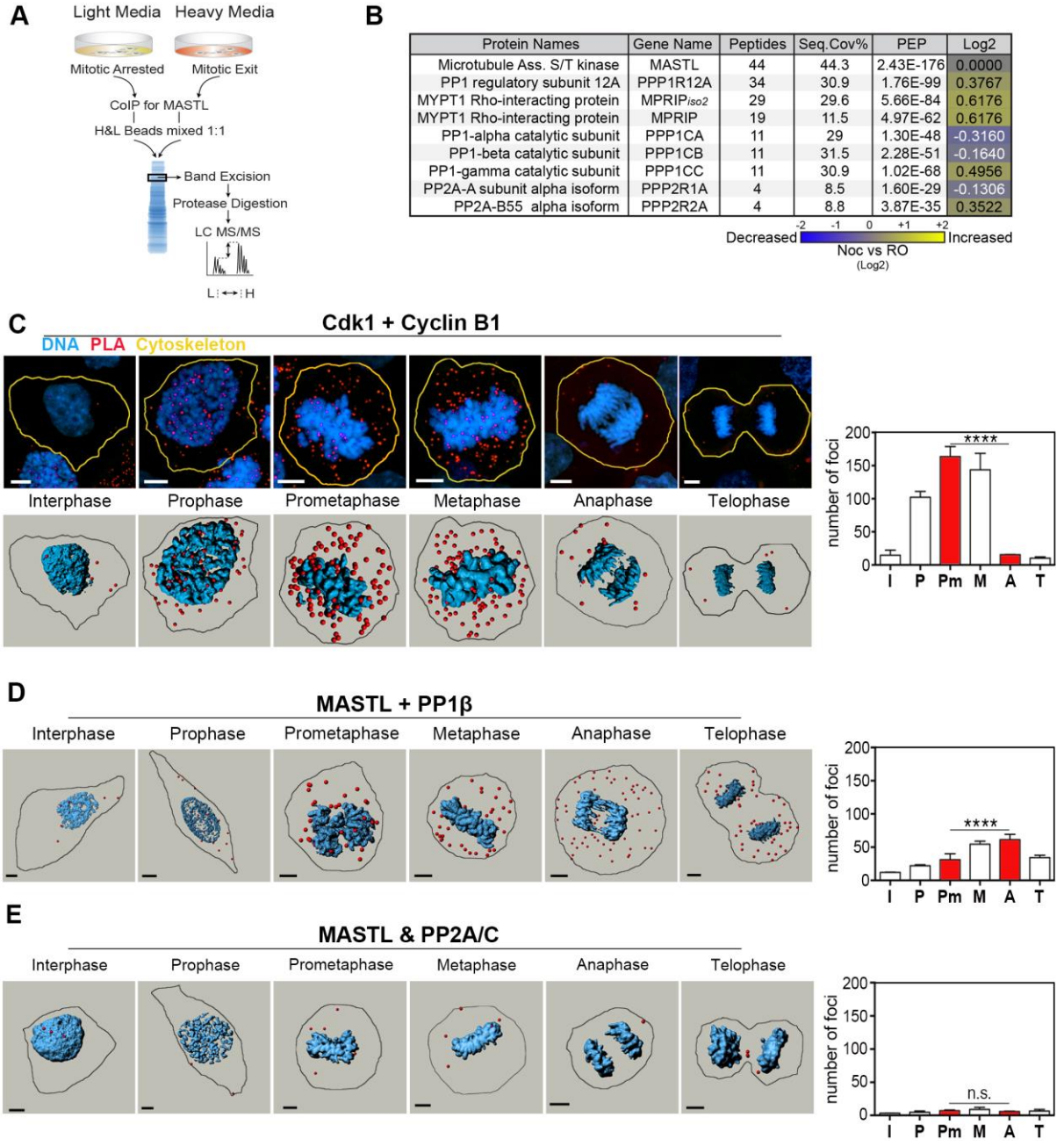

Figure 3. MASTL binds to protein phosphatase-1 during mitotic exit. [A] Schematic of SILAC labelling, CoIP, and LC-MS/MS analysis of endogenous MASTL. **[B]** Summary table of MaxQuant analysis of 3A showing phosphatases associated with MASTL, posterior error probability (PEP), and $\log_2$ heavy:light ratios (Log2). **[C-E]** Representative maximum projections (**[C]** only) and rendered 3D images of PLA using primary antibody pairs against **[C]** Cdk1 & Cyclin B1 (control), **[D]** MASTL & PP1β, and **[E]** MASTL & PP2A/C.

Individual PLA dots were quantified using Imaris dot counter across interphase (I), prophase (P), prometaphase (Pm), metaphase (M), anaphase (A), and telophase (T). Prometaphase and anaphase were compared (red bars) for $n > 5$ cells, across 2 replicates. P-values ****=<0.00001, n.s.= not significant (two-way ANOVA) (scale bars = 10 μm).

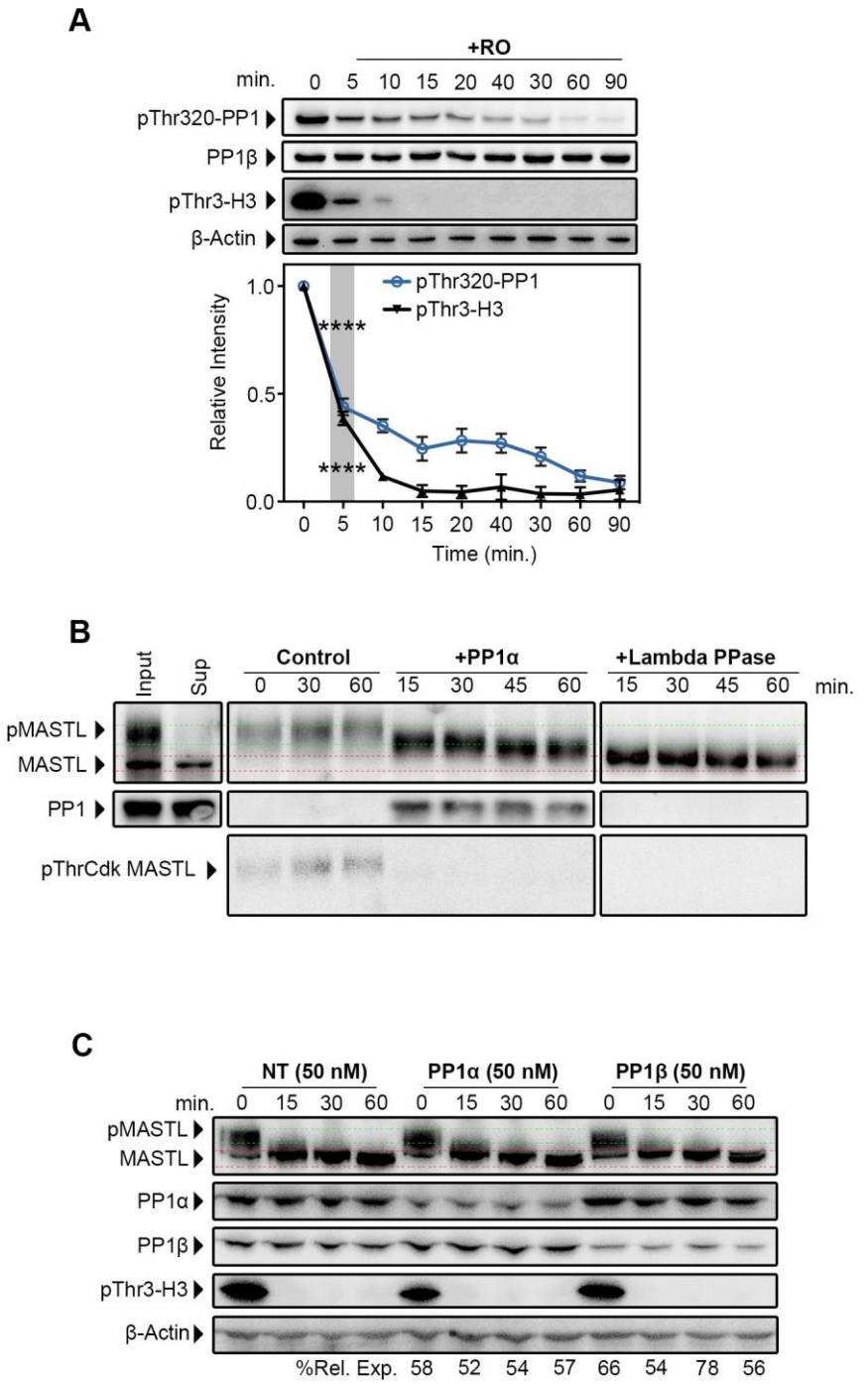

Figure 4. PP1 is rapidly activated during exit and capable of partially dephosphorylating MASTL *in vitro*. [A] Lysates as per Fig. 1B were blotted for PP1 phosphorylated on Thr320 (pThr320-PP1), total PP1β, the PP1 substrate histone H3 phosphorylated on Thr3 (pThr3-H3), and β-actin (loading). Quantification relative to 0 min. time point (mean + s.e.m.) for n=3 P-values ****<0.001 (one-way ANOVA). **[B]** MASTL

immunoprecipated from mitotic HeLa extracts, treated with Okadaic acid, and incubated with recombinant PP1α or Lambda phosphatase (Lambda PPase) or without (control) for the indicated time-points. Samples analysed by western blot. Phosphorylation of MASTL assessed by band shift and pThrCdk. **[C]** HeLa cells transfected with 50nM of siRNA against PP1α, PP1β or a non-targeting control (NT) for 24 h. Cells were then treated as Fig. 1A. Dephosphorylation of MASTL was analysed by band-shift, PP1 activity measured by pThr3-H3 dephosphorylation. Values indicate percentage of PP1α, PP1β remaining after knockdown relative to control.

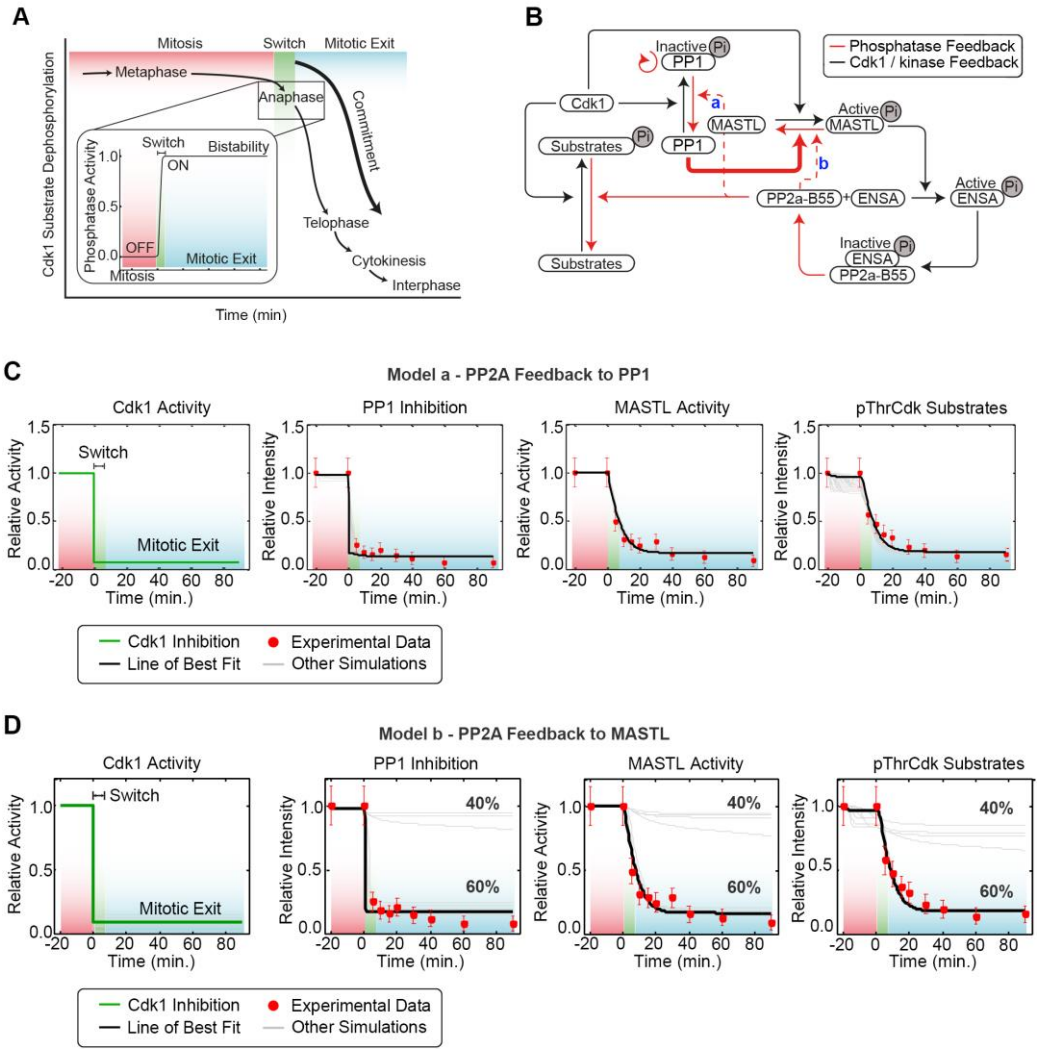

Figure 5. The bistability of mitotic exit can be modelled using observed experimental parameters. [A] A model of the bistable phosphatase activity during mitosis, with repression (red shading) during metaphase, and activation (blue shading) separated by the bistable switch (green shading). **[B]** Schematic of the mathematical model, with dephosphorylation of MASTL by PP1 (bold red line), feedback from PP2A (dotted red line) onto either; PP1 (model (a)), or MASTL (model (b)). **[C, D]** Optimized mathematical model where; **[C]** Model (a) fitted to training data from 50 independent parameter estimation runs. Best fit (black line) depicts 91.1% Cdk1 inhibition. **[D]** Model (b) 60% of the simulations run accurately fit experimental data.

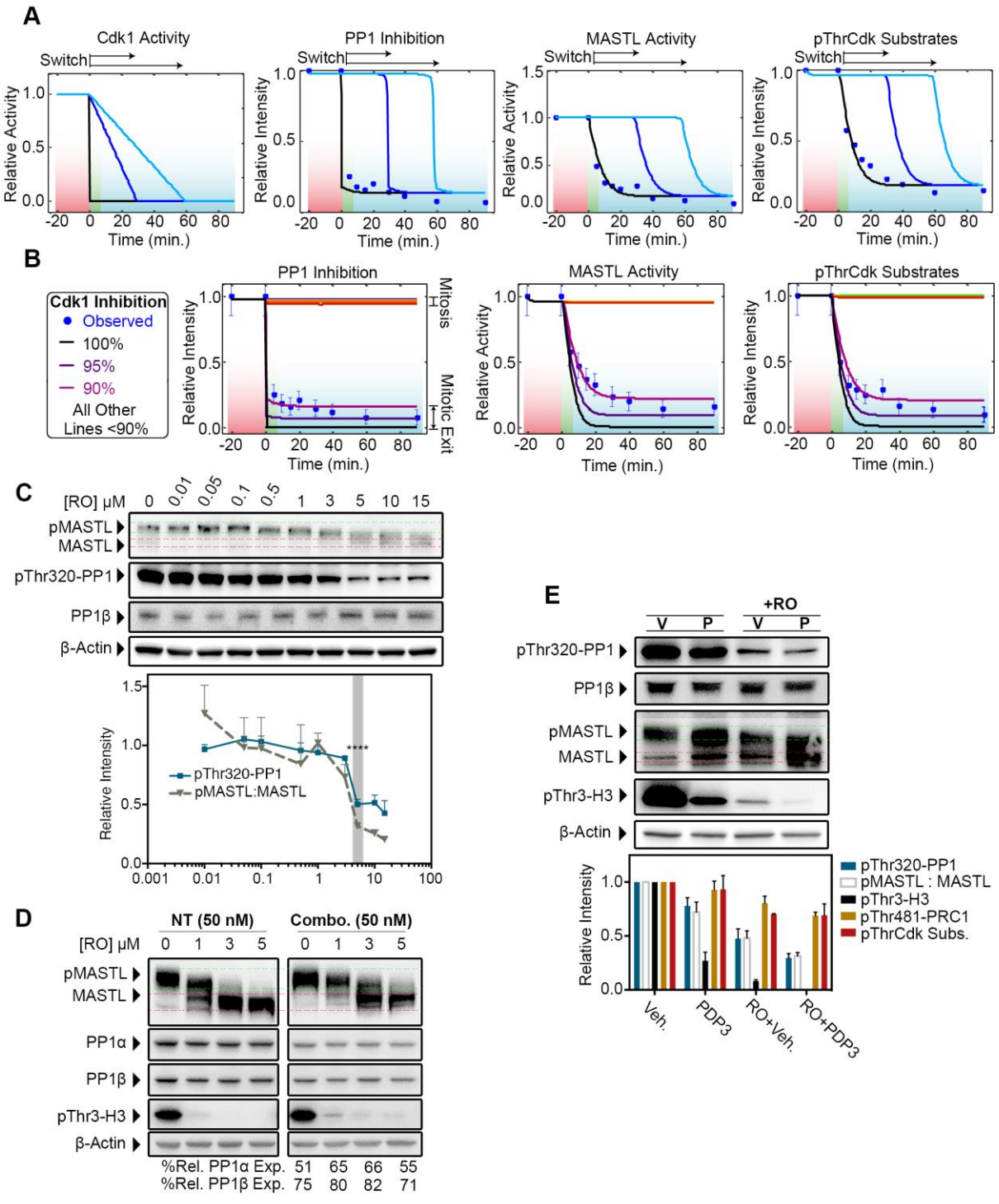

Figure 6. A threshold of Cdk1 activity, and PP1 are required to trigger the mitotic exit switch. [A] Rate of Cdk1 inhibition from model (a), was changed to 2 different linear decay rates (blue lines), and subsequent effects on PP1 inhibition, MASTL activity, and pThrCdk substrate dephosphorylation modelled. **[B]** Inhibition of Cdk1 was varied from 5-100%, in

5% increments using model (a). **[C]** Validation of Cdk1 bistability threshold. Whole cell lysates treated with RO for 15 min were probed by western blot for total PP1β, pThr320-PP1, and MASTL. Shown are representative blots, quantification (mean + s.e.m.) for n = 3, MASTL activity was estimated by quantifying the ratio (pMASTL:MASTL) of pMASTL (green lines) to MASTL (red lines), bistability is highlighted (grey shading) (ordinary one-way ANOVA), ****= $P < 0.0001$. **[D]** HeLa cells co-depleted of PP1α (25 nM) and PP1β (25 nM) (combo) or with non-targeting (control) siRNA were synchronised, as per 1A, treated with increasing concentrations of RO3306 (RO) for 30 min, and assessed by western blot for knockdown efficency, dephosphorylation of MASTL (band-shift), and PP1 substrate pThr3-H3. Values represent amount of PP1α and β remaining, relative to control treatments. n=2. **[E]** HeLa cells were synchronised as per Fig. 1A, but treated with the PP1 activating peptide PDP3 (40 μM, P) or vehicle (V) control for 3 hrs prior to harvest. Samples were treated with (+RO) or without 3 μM RO3306 for 30 min. Lysates were analysed by western blot and quantified relative to vehicle (far left lane), for pThr320-PP1, total PP1β, MASTL, pThr3-H3, and β-Actin (see Fig. S4B for pThr481-PRC1 and pThrCdk Substrates), n = 2.

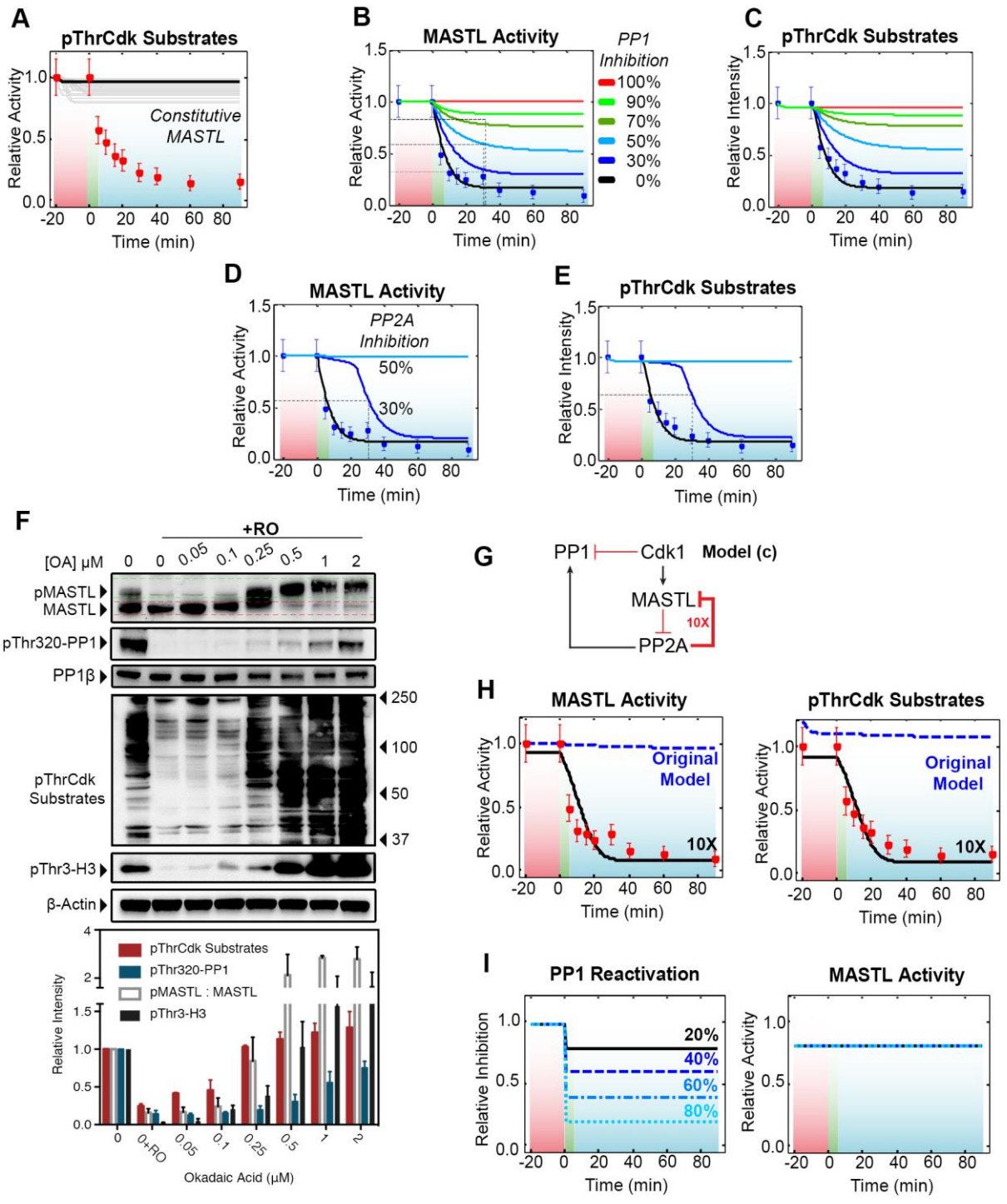

Figure 7. PP2A-PP1 feedback is critical for ultra-sensitivity and bistability. [A] Effects of constitutively active MASTL on mitotic exit were simulated 50 times (grey lines) using model a. **[B, C]** Using Model (a) the effect of PP1 inhibition on MASTL activity and

pThrCdk substrates was simulated. Removal of the PP1 auto-dephosphorylation loop (red line) completely abolished PP1 activity, disrupting bistability. Simulating partial inhibition of PP1 activity from 30-90% (blue and green lines) by reducing k2 (see k2b Fig. S3F) resulted in a corresponding increase in relative activity of MASTL and pThrCdk phosphorylation. **[D, E]** Similar to A & B, except the effects of PP2A inhibition on MASTL and pThrCdk substrate phosphorylation were simulated by reducing k4 (see k4b Fig. S3F) as measured by MASTL activity and pThrCdk substrates. **[F]** HeLa cells synchronised as per Fig. 1A, were treated for 1 h with increasing doses of the PP1/PP2A inhibitor Okadaic acid (OA) followed by 10 μM RO for 30 min. Total cell lysates were analysed by western blot and quantified for total PP1β, pThr320-PP1, pMASTL:MASTL, pThr3-H3 and pThrCdk substrates as a measure of mitotic exit and bistability, for $n = 2$. **[G]** Schematic of the final model (c) which lacks the dephosphorylation of MASTL by PP1. **[H]** Model (a rev) (dotted blue line) is unable to trigger MASTL dephosphorylation, or pThrCdk substrate dephosphorylation, unless PP2A feedback on MASTL is amplified 10-fold (model (c), bold red line). **[I]** In model (c) PP1 is activated in varying amounts (black, and blue lines) in place of Cdk1 inhibition, and the effect is measured on MASTL activity.

References

Bettencourt-Dias, M., Giet, R., Sinka, R., Mazumdar, A., Lock, W. G., Balloux, F., Zafiropoulos, P. J., Yamaguchi, S., Winter, S., Carthew, R. W., et al. (2004). Genome-wide survey of protein kinases required for cell cycle progression. *Nature* **432**, 980–987.

Blake-Hodek, K. A., Williams, B. C., Zhao, Y., Castilho, P. V., Chen, W., Mao, Y., Yamamoto, T. M. and Goldberg, M. L. (2012). Determinants for activation of the atypical AGC kinase Greatwall during M phase entry. *Mol. Cell. Biol.* **32**, 1337–1353.

Bouchoux, C. and Uhlmann, F. (2011). A Quantitative Model for Ordered Cdk Substrate Dephosphorylation during Mitotic Exit. *Cell* **147**, 803–814.

Browne, B. C., Hochgräfe, F., Wu, J., Millar, E. K. A., Barraclough, J., Stone, A., McCloy, R. A., Lee, C. S., Roberts, C., Ali, N. A., et al. (2013). Global characterization of signalling networks associated with tamoxifen resistance in breast cancer. *FEBS J.* **280**, 5237–5257.

Burgess, A., Lorca, T. and Castro, A. (2012). Quantitative live imaging of endogenous DNA replication in mammalian cells. *PLoS ONE* **7**, e45726.

Burgess, A., Vigneron, S., Brioudes, E., Labbé, J. C., Lorca, T. and Castro, A. (2010). Loss of human Greatwall results in G2 arrest and multiple mitotic defects due to deregulation of the cyclin B-Cdc2/PP2A balance. *PNAS* **107**, 12564–12569.

Chang, D. C., Xu, N. and Luo, K. Q. (2003). Degradation of cyclin B is required for the onset of anaphase in Mammalian cells. *Journal of Biological Chemistry* **278**, 37865–37873.

Chatterjee, J., Beullens, M., Sukackaite, R., Qian, J., Lesage, B., Hart, D. J., Bollen, M. and Köhn, M. (2012). Development of a Peptide that Selectively Activates Protein Phosphatase-1 in Living Cells. *Angewandte Chemie International Edition* **51**, 10054–10059.

Cundell, M. J., Bastos, R. N., Zhang, T., Holder, J., Gruneberg, U., Novák, B. and Barr, F. A. (2013). The BEG (PP2A-B55/ENSA/Greatwall) pathway ensures cytokinesis follows chromosome separation. *Mol. Cell* **52**, 393–405.

Di Virgilio, M., Callen, E., Yamane, A., Zhang, W., Jankovic, M., Gitlin, A. D., Feldhahn, N., Resch, W., Oliveira, T. Y., Chait, B. T., et al. (2013). Rif1 prevents resection of DNA breaks and promotes immunoglobulin class switching. *Science* **339**, 711–715.

El-Armouche, A., Bednorz, A., Pamminger, T., Ditz, D., Didié, M., Dobrev, D. and Eschenhagen, T. (2005). Role of calcineurin and protein phosphatase-2A in the regulation of phosphatase inhibitor-1 in cardiac myocytes. *Biochem. Biophys. Res. Commun.* **346**, 700–706.

Favre, B., Turowski, P. and Hemmings, B. A. (1997). Differential inhibition and posttranslational modification of protein phosphatase 1 and 2A in MCF7 cells treated with calyculin-A, okadaic acid, and tautomycin. *Journal of Biological Chemistry* **272**, 13856–13863.

Gavet, O. and Pines, J. (2010). Progressive activation of CyclinB1-Cdk1 coordinates entry to mitosis. *Dev Cell* **18**, 533–543.

Gharbi-Ayachi, A., Labbé, J. C., Burgess, A., Vigneron, S., Strub, J.-M., Brioudes, E., Van-Dorsselaer, A., Castro, A. and Lorca, T. (2010). The substrate of Greatwall kinase, Arpp19, controls mitosis by inhibiting protein phosphatase 2A. *Science* **330**, 1673–1677.

Grallert, A., Boke, E., Hagting, A., Hodgson, B., Connolly, Y., Griffiths, J. R., Smith, D. L., Pines, J. and Hagan, I. M. (2014). A PP1–PP2A phosphatase relay controls mitotic progression. *Nature* **517**, 94–98.

Heim, A., Konietzny, A. and Mayer, T. U. (2015). Protein phosphatase 1 is essential for Greatwall inactivation at mitotic exit. *EMBO Rep*.

Hengl, S., Kreutz, C., Timmer, J. and Maiwald, T. (2007). Data-based identifiability analysis of non-linear dynamical models. *Bioinformatics* **23**, 2612–2618.

Hégarat, N., Vesely, C., Vinod, P. K., Ocasio, C., Peter, N., Gannon, J., Oliver, A. W., Novák, B. and Hochegger, H. (2014). PP2A/B55 and Fcp1 regulate Greatwall and Ensa dephosphorylation during mitotic exit. *PLoS Genet.* **10**, e1004004.

Ingber, L. (1989). Very fast simulated re-annealing. *Mathematical and Computer Modelling* **12**, 967–973.

Kolker, E., Higdon, R., Haynes, W., Welch, D., Broomall, W., Lancet, D., Stanberry, L. and Kolker, N. (2012). MOPED: Model Organism Protein Expression Database. *Nucleic Acids Res.* **40**, D1093–9.

Kwon, Y. G., Lee, S. Y., Choi, Y., Greengard, P. and Nairn, A. C. (1997). Cell cycle-dependent phosphorylation of mammalian protein phosphatase 1 by cdc2 kinase. *PNAS* **94**, 2168–2173.

Lindqvist, A., Rodriguez-Bravo, V. and Medema, R. H. (2009). The decision to enter mitosis: feedback and redundancy in the mitotic entry network. *J. Cell Biol.* **185**, 193–202.

Lontay, B., Kiss, A., Gergely, P., Hartshorne, D. J. and Erdődi, F. (2005). Okadaic acid induces phosphorylation and translocation of myosin phosphatase target subunit 1 influencing myosin phosphorylation, stress fiber assembly and cell migration in HepG2 cells. *Cell Signal* **17**, 1265–1275.

López-Avilés, S., Kapuy, O., Novák, B. and Uhlmann, F. (2009). Irreversibility of mitotic exit is the consequence of systems-level feedback. *Nature* **459**, 592–595.

Maiwald, T. and Timmer, J. (2008). Dynamical modeling and multi-experiment fitting with PottersWheel. *Bioinformatics* **24**, 2037–2043.

McCloy, R. A., Parker, B. L., Rogers, S., Chaudhuri, R., Gayevskiy, V., Hoffman, N. J., Ali, N., Watkins, D. N., Daly, R. J., James, D. E., et al. (2015). Global Phosphoproteomic Mapping of Early Mitotic Exit in Human Cells Identifies Novel Substrate Dephosphorylation Motifs. *Mol. Cell Proteomics* **14**, 2194–2212.

McCloy, R. A., Rogers, S., Caldon, C. E., Lorca, T., Castro, A. and Burgess, A. (2014). Partial inhibition of Cdk1 in G 2 phase overrides the SAC and decouples mitotic events. *Cell Cycle* **13**, 1400–1412.

Medema, R. H. and Lindqvist, A. (2011). Boosting and suppressing mitotic phosphorylation. *Trends in Biochemical Sciences* **36**, 578–584.

Mitchell, N. J., Malins, L. R., Liu, X., Thompson, R. E., Chan, B., Radom, L. and Payne, R. J. (2015). Rapid Additive-Free Selenocystine-Selenoester Peptide Ligation. *J. Am. Chem. Soc.* **137**, 14011–14014.

Mocciaro, A. and Schiebel, E. (2010). Cdc14: a highly conserved family of phosphatases with non-conserved functions? *J Cell Sci* **123**, 2867–2876.

Mochida, S., Ikeo, S., Gannon, J. and Hunt, T. (2009). Regulated activity of PP2A–B55δ is crucial for controlling entry into and exit from mitosis in Xenopus egg extracts. *The EMBO Journal* **28**, 2777–2785.

Mochida, S., Maslen, S. L., Skehel, M. and Hunt, T. (2010). Greatwall phosphorylates an inhibitor of protein phosphatase 2A that is essential for mitosis. *Science* **330**, 1670–1673.

Qian, J., Lesage, B., Beullens, M., Van Eynde, A. and Bollen, M. (2011). PP1/Repo-man dephosphorylates mitotic histone H3 at T3 and regulates chromosomal aurora B targeting. *Curr. Biol.* **21**, 766–773.

Rattani, A., Vinod, P. K., Godwin, J., Tachibana-Konwalski, K., Wolna, M., Malumbres, M., Novák, B. and Nasmyth, K. (2014). Dependency of the spindle assembly checkpoint on Cdk1 renders the anaphase transition irreversible. *Curr. Biol.* **24**, 630–637.

Reither, G., Chatterjee, J., Beullens, M., Bollen, M., Schultz, C. and Köhn, M. (2013). Chemical activators of protein phosphatase-1 induce calcium release inside intact cells. *Chem Biol* **20**, 1179–1186.

Rogers, S., Gloss, B. S., Lee, C. S., Sergio, C. M., Dinger, M. E., Musgrove, E. A., Burgess, A. and Caldon, C. E. (2015a). Cyclin E2 is the predominant E-cyclin associated with NPAT in breast cancer cells. *Cell Division* **10**, 1.

Rogers, S., McCloy, R. A., Parker, B. L., Chaudhuri, R., Gayevskiy, V., Hoffman, N. J., Watkins, D. N., Daly, R. J., James, D. E. and Burgess, A. (2015b). Dataset from the global phosphoproteomic mapping of early mitotic exit in human cells. *Data Brief* **5**, 45–52.

Schmitz, M. H. A., Held, M., Janssens, V., Hutchins, J. R. A., Hudecz, O., Ivanova, E., Goris, J., Trinkle-Mulcahy, L., Lamond, A. I., Poser, I., et al. (2010). Live-cell imaging RNAi screen identifies PP2A-B55alpha and importin-beta1 as key mitotic exit regulators in human cells. *Nat Cell Biol* **12**, 886–893.

Thomson, M. and Gunawardena, J. (2009). Unlimited multistability in multisite phosphorylation systems. *Nature* **460**, 274–277.

Tóth, A., Queralt, E., Uhlmann, F. and Novák, B. (2007). Mitotic exit in two dimensions. *J. Theor. Biol.* **248**, 560–573.

Vassilev, L. T., Tovar, C., Chen, S., Knezevic, D., Zhao, X., Sun, H., Heimbrook, D. C. and Chen, L. (2006). Selective small-molecule inhibitor reveals critical mitotic functions of human CDK1. *PNAS* **103**, 10660–10665.

Vera, J., Lartigue, L., Vigneron, S., Gadéa, G., Gire, V., Del Rio, M., Soubeyran, I., Chibon, F., Lorca, T. and Castro, A. (2015). Greatwall promotes cell transformation by hyperactivating AKT in human malignancies. *Elife* **4**, e10115.

Verdugo, A., Vinod, P. K., Tyson, J. J. and Novák, B. (2013). Molecular mechanisms creating bistable switches at cell cycle transitions. *Open Biol* **3**, 120179–120179.

Vigneron, S., Brioudes, E., Burgess, A., Labbé, J. C., Lorca, T. and Castro, A. (2009). Greatwall maintains mitosis through regulation of PP2A. *The EMBO Journal* **28**, 2786–2793.

Vigneron, S., Gharbi-Ayachi, A., Raymond, A.-A., Burgess, A., Labbé, J. C., Labesse, G., Monsarrat, B., Lorca, T. and Castro, A. (2011). Characterization of the mechanisms controlling Greatwall activity. *Mol. Cell. Biol.* **31**, 2262–2275.

Williams, B. C., Filter, J. J., Blake-Hodek, K. A., Wadzinski, B. E., Fuda, N. J., Shalloway, D. and Goldberg, M. L. (2014). Greatwall-phosphorylated Endosulfine is both an inhibitor and a substrate of PP2A-B55 heterotrimers. *Elife* **3**, e01695.

Wolf, F., Wandke, C., Isenberg, N. and Geley, S. (2006). Dose-dependent effects of stable cyclin B1 on progression through mitosis in human cells. *The EMBO Journal* **25**, 2802–2813.

Wu, J. Q., Guo, J. Y., Tang, W., Yang, C.-S., Freel, C. D., Chen, C., Nairn, A. C. and Kornbluth, S. (2009). PP1-mediated dephosphorylation of phosphoproteins at mitotic exit is controlled by inhibitor-1 and PP1 phosphorylation. *Nat Cell Biol* **11**, 644–651.

Yamamoto, T. M., Blake-Hodek, K., Williams, B. C., Lewellyn, A. L., Goldberg, M. L. and Maller, J. L. (2011). Regulation of Greatwall kinase during Xenopus oocyte maturation. *Mol. Biol. Cell* **22**, 2157–2164.

Yamamoto, T. M., Wang, L., Fisher, L. A., Eckerdt, F. D. and Peng, A. (2014). Regulation of Greatwall kinase by protein stabilization and nuclear localization. *Cell Cycle* **13**, 0–3575.

Yang, Q. and Ferrell, J. E. (2013). The Cdk1-APC/C cell cycle oscillator circuit functions as a time-delayed, ultrasensitive switch. *Nat Cell Biol* **15**, 519–525.

Supplementary Figures

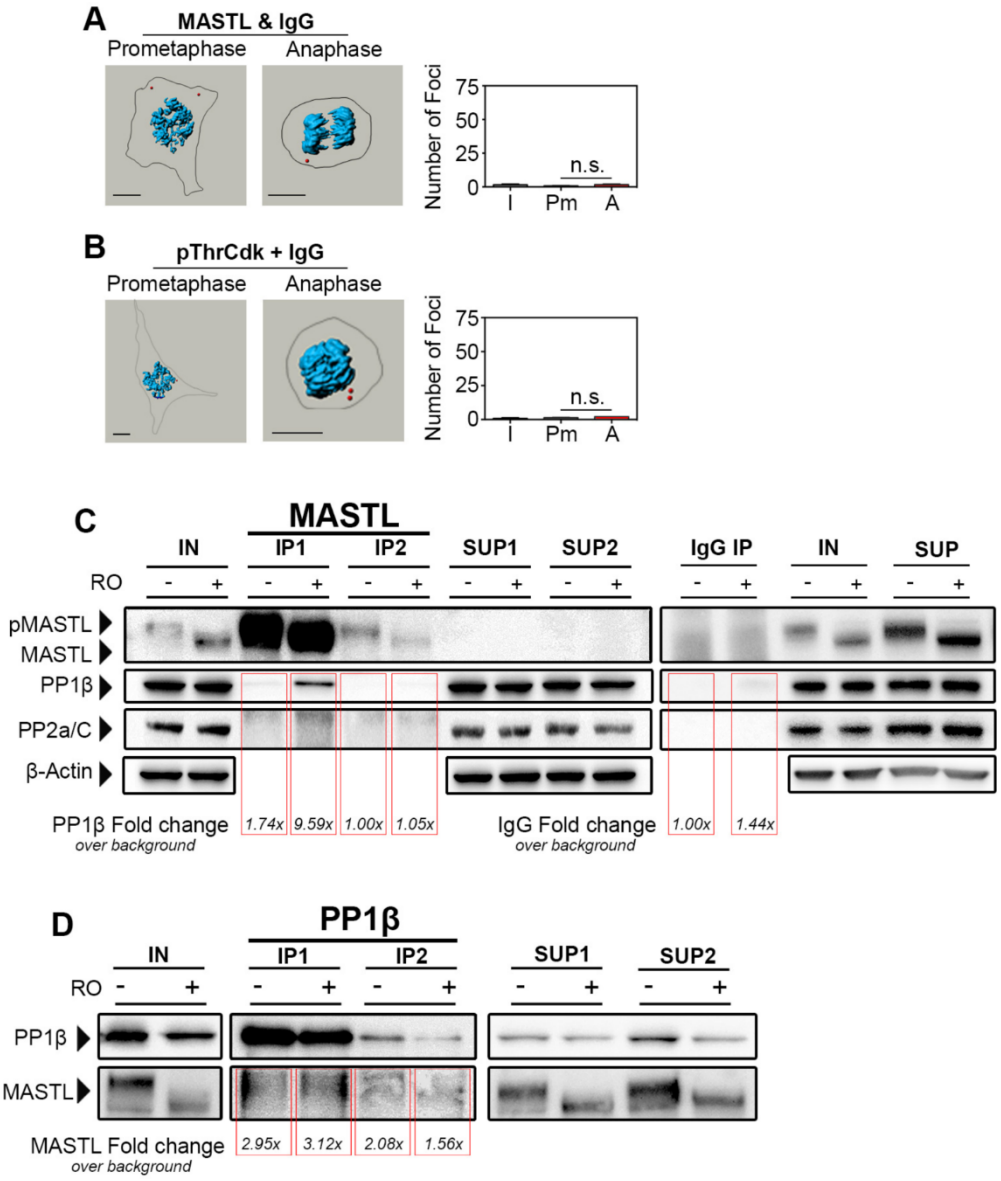

Supplementary Figure 1. Control proximity ligation assay, and CoIP for MASTL and PP1. Naturally cycling fixed, and permeabilised HeLa cells were incubated with either; **[A]** MASTL, or **[B]** pThrCdk Substrate antibodies along with normal rabbit IgG and then processed according the PLA kit, the micrographs containing the fluorescent dots were rendered in Imaris (scale bars indicate 10 µm), for $n = 5$ cells minimum, P-value n.s.= not significant (one-way ANOVA). **[C]** Lysates (IN) either arrested with nocodazole (-RO) or treated with RO3306 (+RO) for 20 min. CoIP of MASTL and normal rabbit IgG were (IP1& IgG IP) were performed on these lysates, with the depleted supernates subjected to an additional round of MASTL precipitation (IP2). The CoIP, whole cell lysate and IP supernatants (SUP1&2) were analysed by western blot. **[D]** similar to A, except lysates were depleted using PP1β antibody.

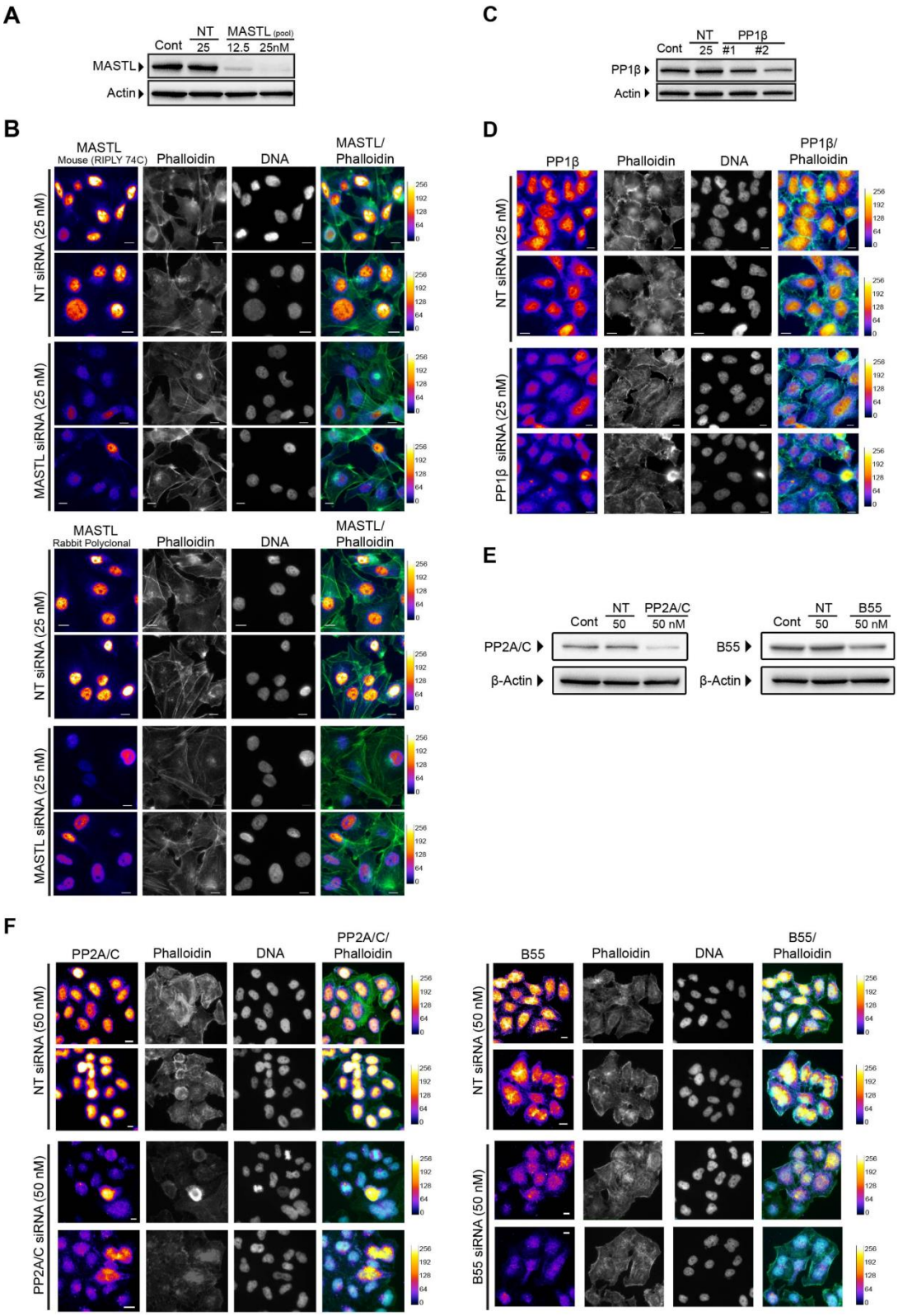

Supplementary Figure 2. Validating MASTL and PP1β antibodies. [A, B] MDA-MB-231 cells were either untransfected (Cont), or transfected for 48 h with non-targeting (NT), or with varying concentrations of MASTL siRNA **[A]** whole cell lysate was analysed by western blot, or **[B]** immunofluorescence, using primary antibodies against MASTL. **[C, D]** HeLa cells were either untransfected (Cont), or transfected for 48 h with non-targeting (NT), or two distinct PP1β siRNA **[C]** whole cell lysate was analysed by western blot, or **[D]** immunofluorescence, using primary antibodies against PP1β.

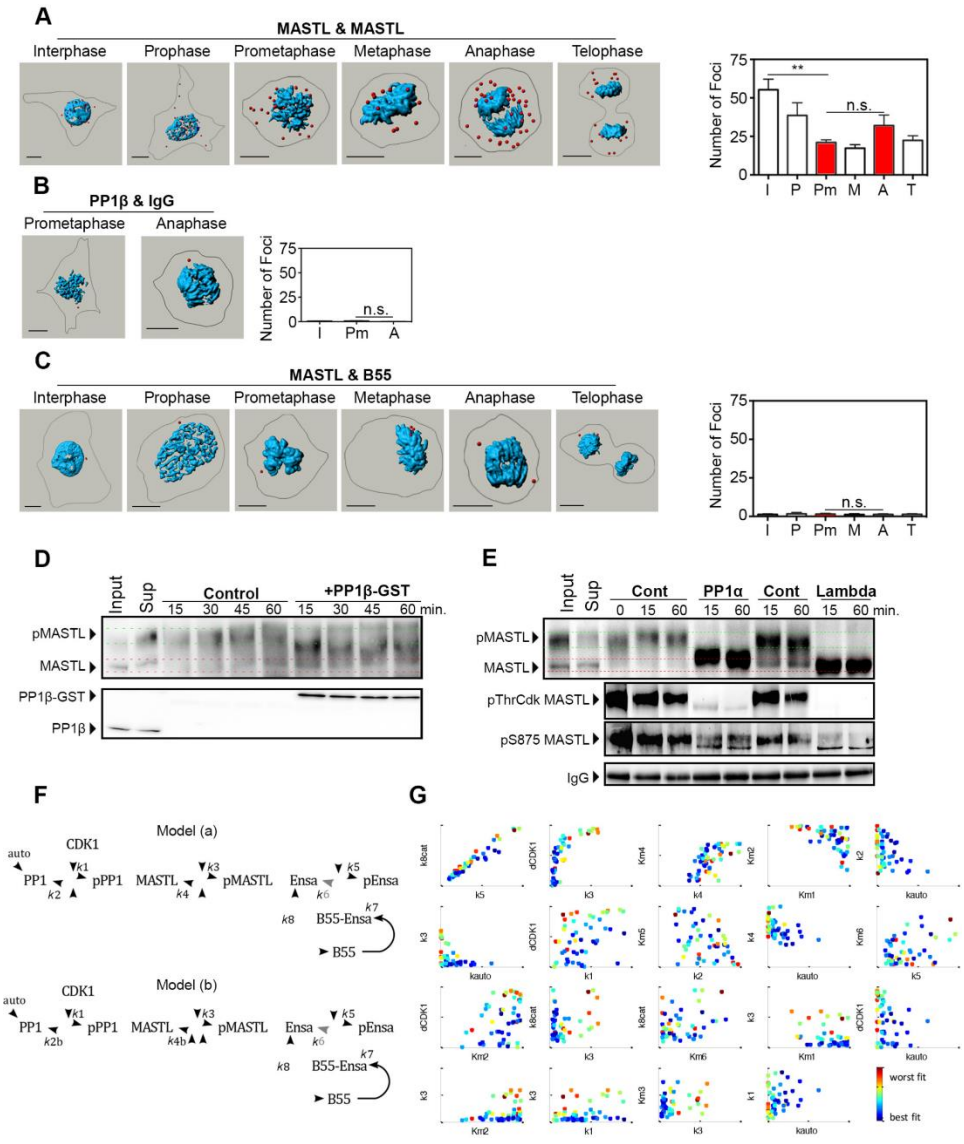

Supplementary Figure 3. Validating PP1 and B55 interactions *in vitro* and *in vivo*. Naturally cycling fixed, and permeabilized HeLa cells were treated with either; **[A]** MASTL mouse & rabbit, or **[B]** PP1β & normal rabbit IgG or, **[C]** MASTL & B55 subunit of PP2A, and then processed according the PLA kit, the micrographs containing the fluorescent dots were counted and rendered in Imaris (scale bars indicate 10 μm), for $n = 5$ cells minimum, P-value **= <0.01, n.s.= not significant (one-way ANOVA). MASTL was IP from Okadaic acid (OA) treated, nocodazole arrested HeLa cells (input) and was either untreated (control) or, treated with; **[D]** recombinant PP1β-GST **[E]** rabbit PP1α, or λ-phosphatase (Lambda), for the indicated times. MASTL phosphorylation was then analysed by western blot for MASTL band-shift, pThrCdk substrate, and pS875 MASTL antibodies. **[F]** The different variations of mathematical models showing the individual parameter numbers for PP2A feedback on PP1 (original, model (a)), PP2A feedback on MASTL (model b), and no PP1 dephosphorylation of MASTL (model (c)). **[G]** graphs showing the estimations of the dependant rate parameters, highlighting the quality of the parameter fit.

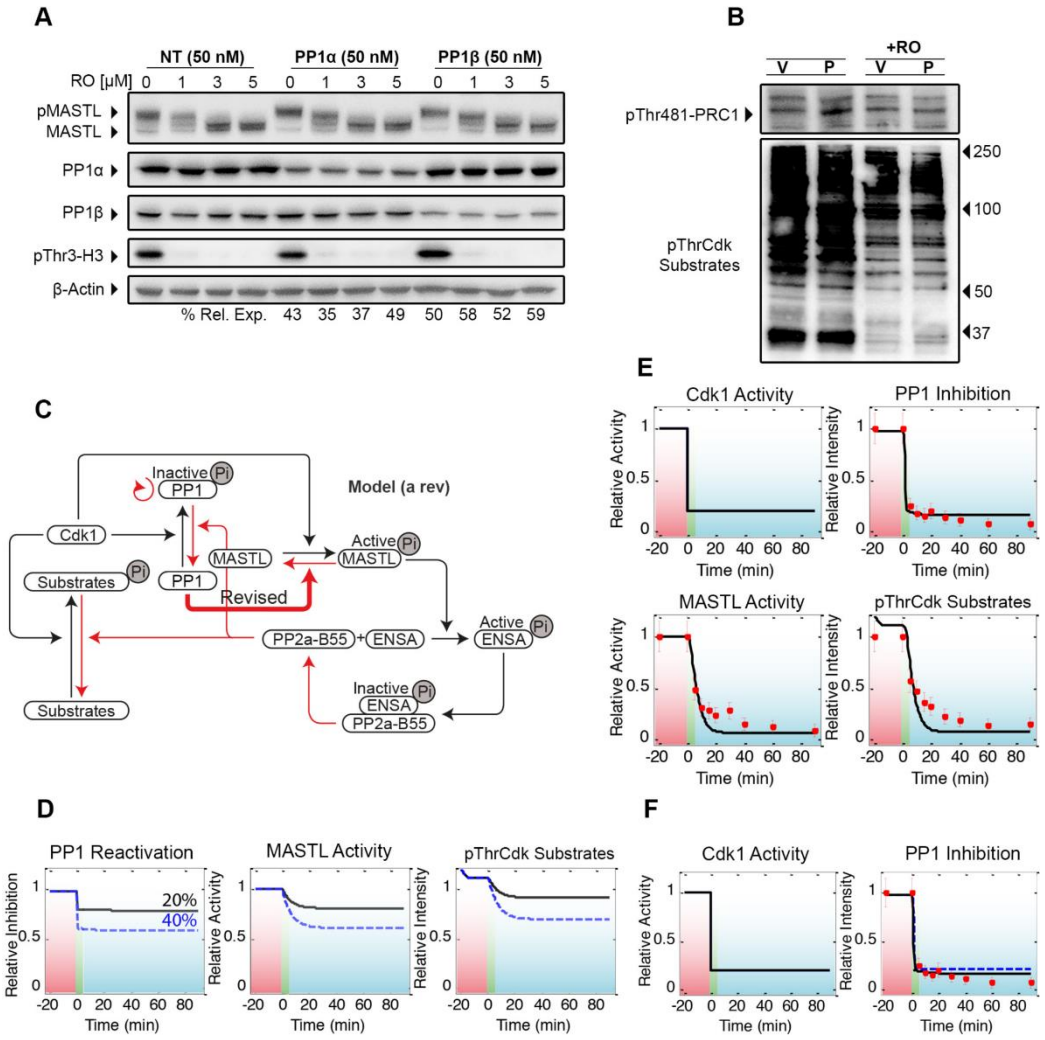

Supplementary Figure 4. PP1 is required to dephosphorylate MASTL and trigger mitotic exit. [A] HeLa cells were transfected with either non-targeting (NT), or PP1α, or PP1β siRNA for 48 h. Cells were then synchronised as per Fig. 1A, and treated with RO3306 for 30 min. at the indicated concentrations. Whole cell lysate was then analysed by western blot for, MASTL band-shift, PP1α, PP1β, pThr3-H3, and β-Actin (loading). Numbers below indicate amount of PP1α/β remaining relative to the respective control knockdown. **[B]** The blots of the PP2A substrates pThr481-PRC1 and pThrCdk Substrates from Fig. 6E. **[C]** Using data generated from the reactivation of PP1 with PDP3 (Fig. 6E) we generated a revised version of our model (a rev, bold red line), where all parameters were re-estimated **[D]** Using model (a rev), we determined the effect of PP1 activation by 20-40% (black and blue lines respectively) under active Cdk1, to assess the effect on MASTL activity, and pThrCdk substrates as validation for the results in Fig. 6E. **[E]** Using model (a rev), we then simulated mitotic exit by inhibiting Cdk1 activity and assessing mitotic exit by PP1 inhibition, MASTL kinase activity, an pThrCdk Substrates. **[F]** Using model (c), Cdk1 activity was inhibited to assess the impact of the revised system on PP1 reactivation.

Supplementary Table S1.

Click here to Download Table S1

Supplementary Table S2. List of ordinary differential equations and initial conditions of the model.

#	Differential equation			Initial condition*
1	d/dt PP1	=	–v1 + v2	0 nM
2	d/dt pPP1	=	v1 – v2	611 nM
3	d/dt Mastl	=	–v3 + v4	0 nM
4	d/dt pMastl	=	v3 – v4	28.6 nM
5	d/dt Ensa	=	–v5 + v6 + v8	0 nM
6	d/dt pEnsa	=	v5 – v6 – v7	100 nM
7	d/dt pEnsaPP2	=	v7 – v8	50 nM
8	d/dt PP2	=	–v7 + v8	0 nM

* Here, the initial conditions correspond to the reported abundances of each protein reports in the MOPED database (Geiger et al., 2012; Kolker et al., 2012). Note that the model was simulated for t<0 min to get the proper mitotic steady-state in untreated conditions (Cdk1=1, see table below) before treatment with Cdk1 inhibitor at t=0 min.

Supplementary Table S3. List of reactions, rate laws and kinetic parameters of the initial model.

#	Reaction	Forward rate	Reverse rate	Parameter values
	i) PP1 phosphorylation and dephosphorylation			
1	PP1 $\xrightarrow{Cdk1}$ pPP1	$\frac{k1\ Cdk1\ PP1}{Km1 + PP1}$		k1 = 91.2 min^{-1} Km1 = 430 nM, see Cdk1 below
2	pPP1 $\xrightarrow{PP2+k_{auto}PP1}$ PP1	$\frac{k2\ (PP2\ + k_{auto}PP1)\ pPP1}{Km2 + pPP1}$		k2 = 73.5 min^{-1}, kauto = 0.353 , Km2 = 370nM
	ii) MASTL phosphorylation and dephosphorylation			
3	Mastl $\xrightarrow{Cdk1}$ pMastl	$\frac{k3\ Cdk1\ Mastl}{Km3 + Mastl}$		k3 = 0.0237 min^{-1} Km3 = 6.73 nM, see Cdk1 below
4	pMastl $\xrightarrow{PP1}$ Mastl	$\frac{k4\ PP1\ pMastl}{Km4 + pMastl}$		k4 = 0.0109 min^{-1} Km4 = 20.1 nM
	iii) ENSA phosphorylation and dephosphorylation			
5	Ensa $\xrightarrow{pGwl}$ pEnsa	$\frac{k5\ pMastl\ Ensa}{Km5 + Ensa}$		k5 = 6.62 min^{-1} Km5 = 30 nM
6	pEnsa ⟶ Ensa	$\frac{k6\ pEnsa}{Km6 + pEnsa}$		k6 = 0.000772 nM min^{-1} Km6 = 27 nM
	iv) ENSA-PP2 interaction			
7	pEnsa + PP2 ⇌ pEnsaPP2	$k7on\ \ pEnsa\ PP2$	$k7off\ \ pEnsaPP2$	k7on = 3.42 min^{-1} nM^{-1} * k7off = 0.408 min^{-1} *
8	pEnsaPP2 ⟶ Ensa + PP2	$k8cat\ pEnsaPP2$		k8cat = 2.88 min^{-1} *

Input: $Cdk1\ = \begin{cases} Cdk1_{tot} & for\ t < 0, \\ Cdk1_{tot}(1 - dCDK1) & for\ t \geq 0, \end{cases}$ $with\ Cdk1_{tot} = 979\ nM,\ dCDK1\ =$ 0.911

* The values for k7on, k7off and k8cat are based on Williams et al. (2014), all other kinetic parameters were estimated based on our time-course data.

Supplementary Table S4. Estimated parameter values.

	k1 (min^{-1})	Km1 (nM)	k2 (min^{-1})	kauto (unitless)	Km2 (nM)	k3 (min^{-1})	Km3 (nM)	k4 (min^{-1})	Km4 (nM)	k5 (min^{-1})	Km5 (nM)	k6 (min^{-1})	Km6 (nM)	k8cat (min^{-1})	dCDK1 (unitless)
Lower and upper bounds	5 100	50 500	5 100	0 2	50 500	0.01 0.25	3 30	0.005 0.050	3 30	1 10	2 50	0.0001 0.0010	2 50	0.5 15.0	0.8 1.0
Best fit	91.2	430	73.5	0.353	370	0.0237	6.73	0.0109	20.1	6.62	30.0	0.000772	27.0	2.88	0.911
Re-estimated best fit	17.1	292	24.8	0.500	422	0.0077	27.9	0.0167	29.8	5.93	16.4	0.0001	12.0	3.13	0.801

Supplementary Table S5.

Click here to Download Table S5

Supplementary Table S6. List of reactions, rate laws and kinetic parameters of the re-estimated model and model versions b and c.

#	Reaction	Forward rate	Reverse rate	Parameter values
	i) PP1 phosphorylation and dephosphorylation			
1	PP1 $\xrightarrow{Cdk1}$ pPP1	$\frac{k1\ Cdk1\ PP1}{Km1 + PP1}$		k1 = 17.1 min^{-1} Km1 = 292 nM, see Cdk1 below
2†	pPP1 $\xrightarrow{PP2+k_{auto}PP1}$ PP1	$\frac{k2\ (PP2\ + k_{auto}PP1)\ pPP1}{Km2 + pPP1}$		k2 = 24.8 min^{-1}, kauto = 0.5 , Km2 = 422 nM
2b	pPP1 $\xrightarrow{k_{auto}PP1}$ PP1	$\frac{k2\ (k_{auto}PP1)\ pPP1}{Km2 + pPP1}$		Same as above for reaction #2
2c	Same as above for reaction #2			
	ii) MASTL phosphorylation and dephosphorylation			
3	Mastl $\xrightarrow{Cdk1}$ pMastl	$\frac{k3\ Cdk1\ Mastl}{Km3 + Mastl}$		k3 = 0.0077 min^{-1} Km3 = 27.9nM, see Cdk1 below
4	pMastl $\xrightarrow{PP1}$ Mastl	$\frac{k4\ PP1\ pMastl}{Km4 + pMastl}$		k4 = 0.0167 min^{-1} Km4 = 29.8 nM
4b	pMastl $\xrightarrow{PP1+PP2}$ Mastl	$\frac{k4\ (PP1\ + PP2)\ pMastl}{Km4 + pMastl}$		Same as above for reaction #4
4c	pMastl $\xrightarrow{PP2}$ Mastl	$\frac{k4\ PP2\ pMastl}{Km4 + pMastl}$		k4 = 0.167 min^{-1} Km4 = 29.8 nM
	iii) ENSA phosphorylation and dephosphorylation			
5	Ensa $\xrightarrow{pGwl}$ pEnsa	$\frac{k5\ pMastl\ Ensa}{Km5 + Ensa}$		k5 = 6.62 min^{-1} Km5 = 30 nM
6	pEnsa ⟶ Ensa	$\frac{k6\ pEnsa}{Km6 + pEnsa}$		k6 = 0.0001 nM min^{-1} Km6 = 12 nM
	iv) ENSA-PP2 interaction			
7	pEnsa + PP2 ⇌ pEnsaPP2	$k7on\ \ pEnsa\ PP2$	$k7off\ \ pEnsaPP2$	k7on = 3.42 min^{-1} nM^{-1} * k7off = 0.408 min^{-1} *
8	pEnsaPP2 ⟶ Ensa + PP2	$k8cat\ pEnsaPP2$		k8cat = 3.13 min^{-1} *

Input: $Cdk1\ = \begin{cases} Cdk1_{tot} & for\ t < 0, \\ Cdk1_{tot}(1 - dCDK1) & for\ t \geq 0, \end{cases}$ $with\ Cdk1_{tot} = 979\ nM,\ dCDK1\ =$ 0.801

* The values for k7on, k7off and k8cat are based on Williams et al. (2014), all other kinetic parameters were estimated based on our time-course data in response to CDK1 inhibition and partial PP1activation.

† Reactions 2 and 4 are used in the original model, reactions 2b,4c and 2c,4c refer to the reactions used in model versions b and c, see Figure 5A and Supplementary Figure 8A and 8D.

Alternative Table layout also indicating which reactions were used in which model.

#	Reaction	Forward rate	Reverse rate	Parameter values	Model a	Model b	Model ar
	i) PP1 phosphorylation and dephosphorylation						
1	PP1 $\xrightarrow{Cdk1}$ pPP1	$\frac{k1\ Cdk1\ PP1}{Km1 + PP1}$		k1 = 17.1 min^{-1} Km1 = 292 nM, see Cdk1 below	x	x	x
2	pPP1 $\xrightarrow{PP2+k_{auto}PP1}$ PP1	$\frac{k2\ (PP2\ + k_{auto}PP1)\ pPP}{Km2 + pPP1}$		k2 = 24.8 min^{-1}, kauto = 0.5 , Km2 = 422 nM	x	-	-
2 b	pPP1 $\xrightarrow{k_{auto}PP1}$ PP1	$\frac{k2\ (k_{auto}PP1)\ pPP1}{Km2 + pPP1}$		Same as above for reaction #2	-	x	
2 c	Same as above for reaction #2				-	-	x
	ii) MASTL phosphorylation and dephosphorylation						
3	Mastl $\xrightarrow{Cdk1}$ pMastl	$\frac{k3\ Cdk1\ Mastl}{Km3 + Mastl}$		k3 = 0.0077 min^{-1} Km3 = 27.9nM, see Cdk1 below	x	x	x
4	pMastl $\xrightarrow{PP1}$ Mastl	$\frac{k4\ PP1\ pMastl}{Km4 + pMastl}$		k4 = 0.0167 min^{-1} Km4 = 29.8 nM	x	x	-
4 b	pMastl $\xrightarrow{PP1+PP2}$ Mastl	$\frac{k4\ (PP1\ + PP2)\ pMastl}{Km4 + pMastl}$		Same as above for reaction #4	-	x	-
4 c	pMastl $\xrightarrow{PP2}$ Mastl	$\frac{k4\ PP2\ pMastl}{Km4 + pMastl}$		k4 = 0.167 min^{-1} Km4 = 29.8 nM	-	-	x
	iii) ENSA phosphorylation and dephosphorylation						
5	Ensa $\xrightarrow{pGwl}$ pEnsa	$\frac{k5\ pMastl\ Ensa}{Km5 + Ensa}$		k5 = 6.62 min^{-1} Km5 = 30 nM	x	x	x
6	pEnsa ⟶ Ensa	$\frac{k6\ pEnsa}{Km6 + pEnsa}$		k6 = 0.0001 nM min^{-1} Km6 = 12 nM	x	x	x
	iv) ENSA-PP2 interaction						
7	pEnsa + PP2 ⇌ pEnsaPP2	$k7on\ pEnsa\ PP2$	$k7off\ pEnsaPP2$	k7on = 3.42 min^{-1} nM^{-1} * k7off = 0.408 min^{-1} *	x	x	x
8	pEnsaPP2 ⟶ Ensa + PP2	$k8cat\ pEnsaPP2$		k8cat = 3.13 min^{-1} *	x	x	x

The x-marks in the last three columns indicate which reactions were used in each of the three different model versions

Supplementary Table S7. All primary, secondary, and conjugated antibodies used

Antibody	Species	Supplier	Cat. #	Dilution Factor
(phospho-Ser-Pro) Cdk Substrates	Rabbit	Cell Signaling	4777	1000
(phospho-Thr-Pro) Cdk Substrates	Mouse	Cell Signaling	9391	1000(WB) 2500 (PLA)
β-Actin	Goat	Santa Cruz	sc-1616	400
Alexa Fluor 488 Goat anti-Rabbit IgG Antibody	Rabbit	Life Technologies	R37116	80
Alexa Fluor 594 Donkey anti-Mouse IgG Antibody	Mouse	Life Technologies	R37115	80
Cdc2 p34 (B-6) (Cdk1)	Mouse	Santa Cruz	sc-8395	100(IF) 200 (WB)
Cyclin B1 (DC510) XP	Rabbit	Cell Signaling	12231	10(IP) 1000(PLA/IF/WB)
HRP-linked Donkey anti-Rabbit IgG Antibody	Rabbit	GE Life Sciences	NA934	1000
HRP-linked Sheep anti-Mouse IgG Antibody	Mouse	GE Life Sciences	NA931	1000
Ku-86	Mouse	Santa Cruz	sc-5280	250
MASTL (Full Length)	Rabbit	Kind Gift A.Castro	n/a	500(IF&PLA) 1000(WB) 4(IP)
MASTL (phospho-Ser875)	Rabbit	Kind Gift A.Castro	n/a	250
MASTL (RIPLY 74C)	Mouse	Abcam	ab166647	50(IF&PLA)
Phospho-PRC1 (Thr481)	Mouse	Santa Cruz	sc-377544	200
phospho-Thr320 PP1α	Rabbit	Cell Signaling	2581	1000
PP1α (FL-18)	Rabbit	Santa Cruz	sc-443	500
PP1β (C-5)	Mouse	Santa Cruz	sc-373782	200
PP2a C-subunit (52F8)	Rabbit	Cell Signaling	2259	100 (WB) 50 (IF/PLA)
PP2A-B55	Rabbit	Cell Signaling	2290	4000(WB) 1000 (IF/PLA)
PRC1 (H-70)	Rabbit	Santa Cruz	sc-8356	200
Rabbit IgG Control (normal rabbit IgG)	Rabbit	Santa Cruz	sc-2027	4(IP) 100(PLA)
Rb (a.a. 332-344)	Mouse	BD Pharmingen	554136	10(IP) 100(PLA) 1000(WB)
Phospho-Rb (Ser780)	Rabbit	Cell Signaling	9307	1000
Securin (DCS-280)	Mouse	Abcam	ab3305	200
β-Actin	Mouse	Sigma Aldrich	A5441	40,000
Phospho-Histone H3 (Thr3)	Rabbit	MerckMillipore	07-424	2500

(WB) = Western Blot (IF) = immunofluorescence (PLA) = proximity ligation assay (IP) = immunoprecipitation.